Interplay between chain stiffness and excluded volume of semiflexible polymers confined in nanochannels

Abhiram Muralidhar,[1] Douglas R. Tree,[1] Yanwei Wang,[2] and Kevin D. Dorfman[1, a)]

[1)] *Department of Chemical Engineering and Materials Science, University of Minnesota – Twin Cities, 421 Washington Avenue SE, Minneapolis, Minnesota 55455, USA*

[2)] *Department of Polymer Science and Engineering, Jiangsu Key Laboratory of Advanced Functional Polymer Design and Application, College of Chemistry, Chemical Engineering and Materials Science, Soochow University, 199 Ren-ai Road, Suzhou 215123, People's Republic of China*

The properties of channel-confined semiflexible polymers are determined by a complicated interplay of chain stiffness and excluded volume effects. Using Pruned-Enriched Rosenbluth Method (PERM) simulations, we study the equilibrium properties of channel-confined polymers by systematically controlling chain stiffness and excluded volume. Our calculations of chain extension and confinement free energy for freely jointed chains with and without excluded volume show excellent agreement with theoretical predictions. For ideal wormlike chains, the extension is seen to crossover from Odijk behavior in strong confinement to zero-stretching, bulk-like behavior in weak confinement. In contrast, for self-avoiding wormlike chains, we always observe that the linear scaling of the extension with the contour length is valid in the long-chain limit irrespective of the regime of confinement, owing to the coexistence of stiffness and excluded volume effects. We further propose that the long-chain limit for the extension corresponds to chain lengths wherein the projection of the end-to-end distance along the axis of the channel is nearly equal to the mean span parallel to the axis. For DNA in nanochannels, this limit was identified using PERM simulations out to molecular weights of more than 1 megabase pairs; the molecular weight of λ-DNA is found to exhibit nearly asymptotic fractional extension for channels sizes used commonly in experiments.

PACS numbers: 87.15.ak, 87.14.gk, 36.20.Cw, 36.20.-r
Keywords: Excluded volume, stiffness, confined polymers, DNA confinement, PERM simulation, nanochannels, Odijk regime, de Gennes regime

[a)]Electronic mail: dorfman@umn.edu

I. Introduction

A long polymer confined inside a narrow channel extends along the channel axis due to constraints imposed by the walls.[1,2]. In weak confinement, where the channel size is somewhat smaller than the polymer's radius of gyration, de Gennes suggested that the resulting chain configuration could be represented by a linearly ordered series of blobs, where the subchain inside the blob obeys self-avoiding random walk statistics.[1,3] Thus, the de Gennes regime arises solely from excluded volume interactions. In strong confinement, where the channel size is small compared to the persistence length of the chain, Odijk proposed that the chain configuration is instead described by a series of deflection segments that obey ideal wormlike chain statistics.[4] In contrast to the de Gennes regime, the Odijk regime produces chain extension even in the absence of excluded volume interactions due to chain stiffness. When viewed in this light, it becomes clear that the Odijk and de Gennes regimes are limiting cases for polymer extension corresponding to the dominance of either chain stiffness or excluded volume.

Unfortunately, neither the Odijk theory nor the de Gennes theory appears to describe the existing experimental data for DNA extension in a nanochannel.[2,5–22] The apparent failure of the classic de Gennes and Odijk theories, when applied to channel-confined DNA, lies in the relative length scales characterizing the DNA experiments; the persistence length of double-stranded DNA ($l_\mathrm{p} \approx 50\,\mathrm{nm}$)[23] is of the same order of magnitude as the channel sizes used in experiments. As a result, the extension of DNA in nanochannel experiments results from a competition between excluded volume effects and chain stiffness for all experimentally relevant channel sizes and molecular weights. For this reason, we recently suggested that it is useful to think of the transition from the Odijk regime to the de Gennes regime as a rod-to-coil transition for the subchain used to renormalize the problem into a series of deflection segments (the rods) or excluded volume de Gennes blobs (the coils).[19] While the details of the physics in the transition region remain a topic of debate, the existence of at least one additional regime between the Odijk and de Gennes regimes now seems very likely.[11,13,17,19,24,25]

In the present contribution, we explore this competition between excluded volume and chain stiffness in considerably more detail than our recent letter.[19] Our exposition is two-fold. In the first part, we use Pruned-Enriched Rosenbluth method (PERM) simulations

of a touching bead model to directly test the Odijk and de Gennes theories within the limits of their underlying assumptions: for the Odijk regime, we consider an ideal wormlike chain; for the de Gennes regime, we consider a self-avoiding, freely jointed chain. So long as the assumptions of the theories are satisfied, we show that their predictions for the chain extension and confinement free energy agree with the simulation data for sufficiently long chains. We also show that our PERM calculations produce the undisputed results for the confinement free energy and extension of an ideal, freely jointed chain. In the second part, we compare the predictions of the chain extension for these idealized cases to the extension of a self-avoiding wormlike chain in a nanochannel as a function of molecular weight and channel size. Our simulations of real wormlike chains clearly produce the Odijk and de Gennes regimes as the limiting cases. Analogous to DNA nanochannel experiments, much of the phase space of our simulations is occupied by chains that satisfy neither theory. We also show that the projection of the end-to-end distance of the confined chain along the channel axis approaches its mean span in the long-chain limit, owing to the difficulty to form hairpins (when stiffness dominates) or the weak penetration of the end of the chain into the linearly ordered, self-avoiding blobs (when excluded volume dominates). We thus propose that the "long-chain" limit corresponds to molecular weights where these two size metrics are approximxately equal; data obtained outside of this limit is subject to artifacts due to finite chain lengths. Remarkably, while recent simulations indicate that λ-DNA (48,500 base pairs, bp) is well below the long-chain limit in free solution ($\sim$ 1 Mbp),[26] the amplification of excluded volume effects in confinement[2] lead to λ-DNA being a sufficiently long chain for most nanochannel experiments measuring the extension.

II. Model and simulation method

A. Discrete wormlike chain model

Consider a wormlike chain of contour length L, persistence length l_{p} and width w confined in a square channel of size D as shown in Fig. 1(a). The length of the channel is much greater than the contour length of the chain and hence there are no end-effects due to finite length of the channel. For simplicity, we assume that the depletion length between the wall and polymer due to excluded volume is $w/2$, which is not necessarily true in general. As a result,

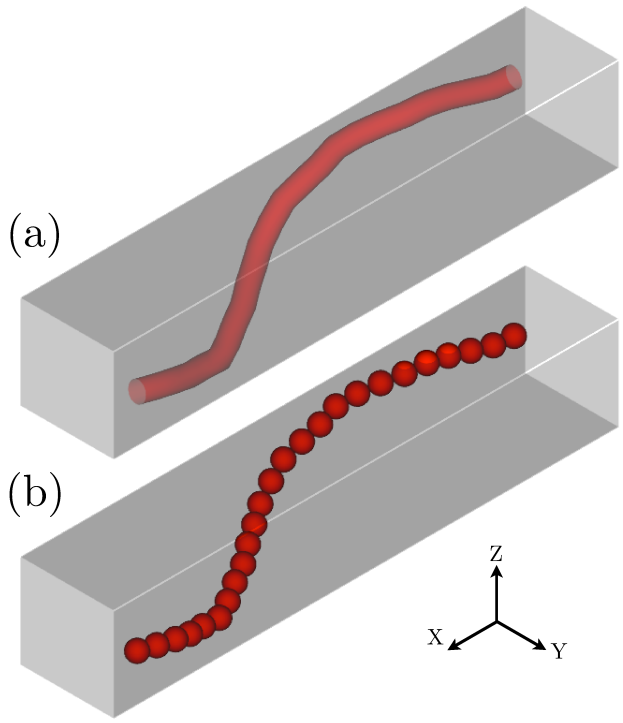

FIG. 1. (a) A WLC with contour length L, persistence length l_{p}, and width w confined in a square channel of size D. (b) Representation of the same chain in our DWLC model. After discretization, the bond length a is set to the value of the width w.

the effective width of the channel accessible to the center of the chain is $D_{\mathrm{eff}} = D - w$.

To carry out the PERM simulations, we use an off-lattice, discrete wormlike chain (DWLC) model.[26,27]. PERM simulations with lattice models have also been successfully used to answer a wide variety of questions surrounding polymer confinement.[28–31] However, these models are known to introduce lattice artifacts, particularly where bending stiffness plays a critical role in determining the properties of the polymer chain.[31] Because our work demands an accurate depiction of chain stiffness in the model, we sacrifice the computational efficiency of a lattice model for the precision of an off-lattice model.

Our model is a touching-bead/necklace model of $N + 1$ beads connected by rigid bonds of length a as shown in Fig. 1(b). Stiffness is imposed by a bending potential given by

$$\beta U_{\mathrm{bend}} = \kappa \sum_{i=1}^{N-1} (1 - \cos\theta_i) \tag{1}$$

between consecutive bonds. The parameter θ_i is the angle between bonds i and $i + 1$, determined by $\cos\theta_i = |\,(\mathbf{r}_{i+2} - \mathbf{r}_{i+1}) \cdot (\mathbf{r}_{i+1} - \mathbf{r}_i)\,|/a^2$, where $\mathbf{r}_k$ is the position vector of the

k^{th} bead. The quantity $\beta = (k_{\text{B}}T)^{-1}$, where k_{B} is the Boltzmann constant and T is the absolute temperature. The bending constant κ is obtained by solving the equation

$$\frac{b}{a} = \frac{\kappa - 1 + \kappa \coth \kappa}{\kappa + 1 - \kappa \coth \kappa}, \tag{2}$$

where $b = 2l_{\text{p}}$ is the Kuhn length of the chain.[26,32]. Note that in the limit $\kappa \to 0$, Eq. 2 reduces to the familiar result for a freely joined chain (FJC), $b = a$. The effect of self-avoidance is incorporated by a hard sphere potential of the form

$$\beta U_{\text{EV}} = \begin{cases} \infty & \text{if } r_{ij} \leq w, \\ 0 & \text{otherwise,} \end{cases} \tag{3}$$

where r_{ij} is the distance between the centers of the beads i and j, and w is the width of the chain.

B. Variants of the DWLC model

In order to investigate the effects of stiffness and excluded volume on properties of confined chains, we adopted a four-step approach in which we independently turned on/off stiffness and excluded volume. Specifically we performed simulations for (i) ideal freely jointed chains (IFJCs); (ii) real freely jointed chains (RFJCs); (iii) ideal wormlike chains (IWLCs) and (iv) real wormlike chains (RWLCs), all confined in square channels of various sizes.

Since the words "ideal" and "real" appear in different contexts in various areas of polymer physics,[33–35] let us clarify what we mean by these terms. We use the word "ideal" to refer to chains in which there are no excluded volume interactions between the beads. In contrast, "real" refers to chains in which there exist repulsive interactions between non-neighboring beads along the contour, as in a polymer dissolved in a good solvent.[33] Thus, a given chain is ideal in the limit $w = 0$, and is real for $w > 0$. Similarly, in the limit $\kappa = 0$, we recover a freely jointed chain (FJC) from the DWLC model, and a wormlike chain (WLC) for $\kappa > 0$.

Note that the term "RFJC model" is somewhat of a misnomer, since one normally assumes that there are no correlations between bond vectors along the contour in a freely jointed chain model.[33–35] The excluded volume interactions do introduce correlations between distal segments of the chain. However, we use the term RFJC to mean that the chain

TABLE I: Presence or absence of stiffness and excluded volume in the four models considered here.

	Bending stiffness (κ)	Excluded volume (w)
Ideal Freely Jointed Chain (IFJC)	$= 0$	$= 0$
Real Freely Jointed Chain (RFJC)	$= 0$	> 0
Ideal Wormlike Chain (IWLC)	> 0	$= 0$
Real Wormlike Chain (RWLC)	> 0	> 0

behaves like a FJC locally, as there is no bending stiffness between different beads of the chain. Therefore, the four kinds of models considered in our work are all special cases of the DWLC model for different values of κ and w. Table I summarizes the properties of the four variants of the DWLC model used here.

C. Pruned-Enriched Rosenbluth Method (PERM) Simulation

As in our previous work,[19,26] we use an off-lattice PERM algorithm to compute equilibrium properties of single polymer chains in confinement. PERM is a Monte Carlo chain-growth algorithm that enables growth of a collection of single polymer molecules which approximately follow a given probability distribution.[36,37] In contrast, the more common Metropolis Monte Carlo (MMC) algorithm employs "moves" in the conformations of a polymer chain of a certain length starting from an initial condition.[38,39] Algorithms based on the Metropolis method are referred to as dynamic Monte Carlo algorithms as they sample states from a Markov chain of states, i.e. a move is chosen probabilistically depending on the previous state.[40] On the other hand, PERM belongs to the class of so-called approximate counting algorithms.[40] Every sample in a PERM simulation consists of a "tour" of configurations grown from a single bead to a maximum of $N+1$ beads. Each step of growth ranging from $i = 0$ to $i = N$ in a tour is associated with a weight W_i, the average $\langle W_i \rangle$ of which is an estimate of the partition function, Z_i, relative to the reference state.

PERM is a powerful technique for single molecule simulation of polymers and has several advantages over conventional MMC methods. First, the free energy of a system (with respect to a reference state) can be estimated directly from the simulation using

$$\beta \Delta F_i = -\ln \frac{Z_i}{Z_{\mathrm{ref},i}} \approx -\ln \left\langle \frac{W_i}{W_{\mathrm{ref},i}} \right\rangle . \tag{4}$$

Here ΔF_i is the free energy of the polymer of length i, and $W_{\mathrm{ref},i}$ and $Z_{\mathrm{ref},i}$ are the weight and the partition function corresponding to the reference state. The average $W_i/W_{\mathrm{ref},i}$ is computed over a total of N_t tours. The reference state we choose in our simulations depends on the variant of the DWLC model under consideration as we explain later in Sec. II D. Second, all equilibrium properties can be estimated as a function of contour length in a single simulation. For example, the mean span X_i at any step i can be estimated as

$$\langle X_i \rangle = \frac{\sum_{t=1}^{N_t} W_i^t X_i^t}{\sum_{t=1}^{N_t} W_i^t}, \tag{5}$$

where W_i^t is the weight associated with the i^{th} step after the t^{th} tour among a maximum of N_t tours. This attribute of PERM of calculating properties as a function of contour length forms the methodological cornerstone of this paper.

Our PERM simulations are based on a parallel master-slave algorithm consisting of three stages, similar to our previous paper:[26] (i) an initial "blind" run to obtain estimates of the partition function for a few hundred beads; (ii) several "non-blind" runs where we incrementally increase the number of beads until the maximum number of beads are reached; (iii) finally, a "full" run wherein properties of interest such as span or end-to-end distance are calculated.[37,41] Our algorithm employs a neighbor list resembling the Verlet list,[42] unlike the hashing-based neighbor lists used in lattice simulations.[36,43,44] Nonetheless, a typical simulation in a given channel with 10^5 beads for 4×10^5 tours running on 96 6-core Intel Xeon X7542 "Westmere" processors takes between 6-8 hours of walltime, which is equivalent to about 700 CPU hours. This large number of tours produce thousands of independent realizations of chains spanning the configuration space, resulting in small error bars. Unless otherwise specified, error bars are smaller than symbol sizes in all our figures. For further details on our implementation of the simulation, we direct the reader to previous work from our group.[19,26]

D. Free energy calculations

In all our simulations, the reference state for the estimation of the partition function is an unconfined chain with no excluded volume. Other attributes of the reference chain, such as a and l_{p}, are set equal to the chain under consideration.[26] In other words, the reference state for simulations of both RWLCs and IWLCs is an unconfined IWLC with the same persistence length. Likewise, the reference state for both IFJCs and RFJCs is an unconfined IFJC.

The confinement free energy of a chain without excluded volume, $\Delta F_{\mathrm{conf,\ id}}$, is calculated by

$$\beta \Delta F_{\mathrm{conf,\ id}} = -\ln \frac{Z_{\mathrm{conf}}}{Z_{\mathrm{ref}}} \approx -\ln \left\langle \frac{W_{\mathrm{conf}}}{W_{\mathrm{ref}}} \right\rangle, \tag{6}$$

where the average of ratio of the weights of the confined chain and the unconfined chain, $W_{\mathrm{conf}}/W_{\mathrm{ref}}$, is evaluated in the course of the simulation. Note that $\langle W_{\mathrm{conf}}/W_{\mathrm{ref}} \rangle$ is an estimate of the ratio of the respective partition functions, $Z_{\mathrm{conf}}/Z_{\mathrm{ref}}$.

Calculation of the confinement free energy of chains with excluded volume involves an additional step as the reference state in our simulations is always an unconfined, ideal chain with the same persistence length. First, the free energy of an unconfined chain with excluded volume, ΔF_{EV}, is obtained from a free-solution PERM simulation by

$$\beta \Delta F_{\mathrm{EV}} = -\ln \frac{Z_{\mathrm{EV}}}{Z_{\mathrm{ref}}} \approx -\ln \left\langle \frac{W_{\mathrm{EV}}}{W_{\mathrm{ref}}} \right\rangle, \tag{7}$$

where Z_{EV} and W_{EV} are the partition function and the weight of the unconfined real chain respectively. Second, the free energy of a confined real chain, $\Delta F_{\mathrm{conf+EV}}$, is calculated through the estimation of the partition function, $Z_{\mathrm{conf+EV}}$, from a PERM simulation of the confined chain as

$$\beta \Delta F_{\mathrm{conf+EV}} = -\ln \frac{Z_{\mathrm{conf+EV}}}{Z_{\mathrm{ref}}} \approx -\ln \left\langle \frac{W_{\mathrm{conf+EV}}}{W_{\mathrm{ref}}} \right\rangle, \tag{8}$$

where $W_{\mathrm{conf+EV}}$ is the corresponding Rosenbluth weight. Finally, the confinement free energy of the real chain, $F_{\mathrm{conf,\ EV}}$, is calculated as

$$\Delta F_{\mathrm{conf,\ EV}} = \Delta F_{\mathrm{conf+EV}} - \Delta F_{\mathrm{EV}}. \tag{9}$$

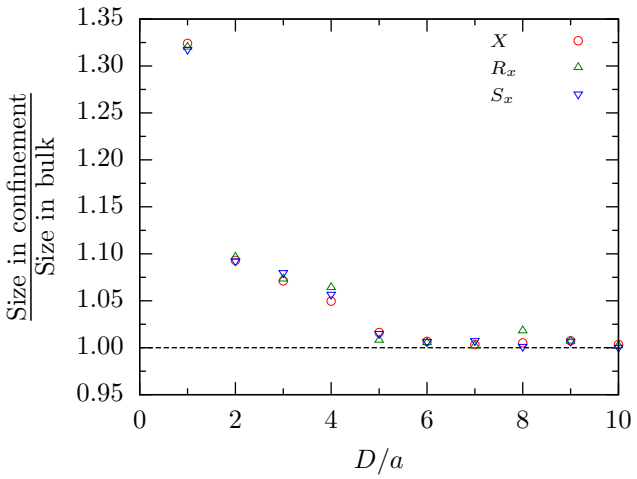

FIG. 2. Mean span (X), x-projection of the end-to-end distance (R_x) and $x-x$ component of the gyration tensor (S_x), normalized by the corresponding quantities in free solution for an ideal FJC, plotted against D/a. The dashed line at unity is the expected result in the absence of discretization error.[1] All data points show simulation results for a contour length $L/a = 5000$.

E. Discretization

Three independent parameters characterize our DWLC model: l_p, w and a. Given l_p and w, the ratios l_p/a and w/a determine the number of discrete units per persistence length and width respectively. By definition, the Kuhn length b must satisfy $b \geq a$, because in the limiting case of a freely joined chain (FJC), we have $b = a$. Moreover, if $w < a$ there is a possibility of the chain crossing itself, and this may result in an erroneous representation of self-repulsion effects. This implies that $w \geq a$. Here, we choose $a = w$,[19] as this yields the best compromise between correct physical representation and computational tractability. In all our chains, $b \geq w$, and hence $a = w$ satisfies the constraints imposed by both stiffness and excluded volume on the bond length.

Channel confinement introduces an additional parameter D, the channel size. A very small D/a ratio can lead to discretization artifacts in the simulation results. In addition, obtaining a reliable number of samples from PERM becomes increasingly difficult as D/a decreases because, for small channels, the attrition rate is high due to collision with walls. Therefore, to determine the role of D/a ratio in our simulations, we calculated the size of ideal FJCs in confinement through PERM simulations.

Here, we make use of the fact that the size of an ideal flexible chain in the direction parallel to the channel is unaffected by confinement.[1] Note that the FJC does not model a

truly "flexible chain" because of the rod-like nature of the model for length scales smaller than the step size, b.[45] However, an unconfined IFJC reproduces the properties of a flexible polymer model such as a continuous Gaussian chain, given that $L \gg b$.[35,45] It is in this context that we use FJC as a model for a flexible polymer. Consequently for an IFJC, we expect that the mean span X,

$$X \equiv \langle \max(x_i) - \min(x_i) \rangle \,, \text{ where } (i \in [1, N+1]), \tag{10}$$

the x-projection of the end-to-end distance R_x,

$$R_x \equiv \sqrt{\left\langle (x_{N+1} - x_1)^2 \right\rangle}, \tag{11}$$

and the $x - x$ component of the gyration tensor S_x,

$$S_x \equiv \sqrt{\left\langle \frac{1}{N+1} \sum_{i=1}^{N+1} (x_i - x_{\text{cm}})^2 \right\rangle} \tag{12}$$

in confinement must be identical to their respective values in free solution. Here, x_i is the x-coordinate of the i^{th} bead, among a total of $N+1$ beads. However, when the bond length is of the order of the confinement size, the assumption that the chain is flexible at the length scale of the channel is no longer valid. Hence the size in confinement is not equal to the size in the bulk.

Figure 2 shows the ratio of these quantities with the corresponding quantities in free solution. As expected, the discretization error increases as D/a decreases. Moreover, for $D/a \geq 5$ there is no significant change in the ratio as D/a increases, and in this region, the ratio of the sizes of the confined and unconfined chains is approximately 1. We use this condition as a rule of thumb to choose the minimum D/a ratio for our simulations of FJCs. Accordingly, all our simulations for FJCs in this paper are done with a ratio $D/a \geq 5$.

III. Results and discussion

In Sec. II B, we classified the DWLC model into 4 broad variants, depending on the values of w and κ. Here in Sec. III A, we examine the properties of confined chains when either

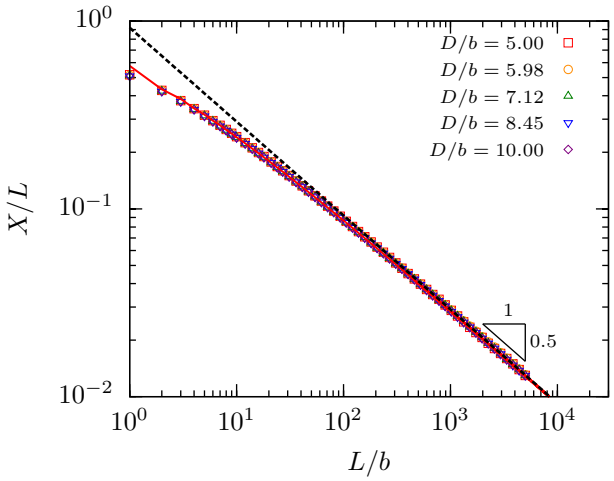

FIG. 3. Average fractional extension as a function of contour length for IFJCs confined in square channels of various sizes. Most data points are not visible as they overlap each other exactly. The red line denotes the theoretical prediction in Eq. 13 for IFJCs in free solution.[46] The dashed line is the result for the mean span in the long-chain limit given by $X = \sqrt{8Lb/3\pi}$.[46] All results show a scaling of $X \sim L^{0.5}$ in the long-chain limit, as expected.

of w or κ (or both) are 0. Thus the limiting cases of no stiffness and no excluded volume encompass (i) IFJCs ($w = 0$ and $\kappa = 0$), (ii) RFJCs ($\kappa = 0$), and (iii) IWLCs ($w = 0$). In Sec. III B, we show simulation results for RWLCs with non-zero values of both w and κ. We then end our discussion in Sec. III B 2 by outlining the implications of our findings to the case of DNA confined in nanochannels.

A. Limiting cases

1. Ideal freely jointed chains (IFJC)

With a carefully discretized DWLC model, we begin with a review of the extension and free energy of ideal flexible chains in confinement. The purpose of laying out the properties of IFJCs is twofold. First, we wish to recapitulate well known results for IFJCs in confinement, which will prove beneficial in elucidating the behavior in the presence of stiffness and excluded volume. Second, because exact analytical results are available for properties of ideal flexible chains in confinement, IFJCs are an ideal candidate for use in validating our simulation code to high precision.

For a flexible ideal chain, confinement does not affect extension parallel to the axis of the channel, i.e. the extension is identical to that in free solution.[1,3] This can be readily

recognized by examining the probability distribution of the end-to-end vectors $\mathbf{R}$ in 3 dimensions, $P_{3D}(N, \mathbf{R})$, for a freely jointed chain with N segments. For an IFJC, the distribution functions in the three orthonormal directions $P_{1D}(N, \mathbf{R}_x)$, $P_{1D}(N, \mathbf{R}_y)$ and $P_{1D}(N, \mathbf{R}_z)$ are independent of each other, i.e., $P_{3D}(N, \mathbf{R}) = P_{1D}(N, \mathbf{R}_x)P_{1D}(N, \mathbf{R}_y)P_{1D}(N, \mathbf{R}_z)$.[35,47] Therefore, for an IFJC confined in a square conduit as in Fig. 1, confinement alters the distribution functions only in the y and z directions. In other words, $P_{1D}^{\text{conf}}(N, \mathbf{R}_x) = P_{1D}^{\text{free}}(N, \mathbf{R}_x)$. Consequently, metrics of size such as the averages of span (X), radius of gyration (S_x) and end-to-end distance (R_x) are unaltered due to confinement.[1,3]

We confirm this prediction by comparing extension of IFJCs confined in channels against the prediction for the mean span of IFJCs in free solution.[46] To do so, we make use of an expression derived by Daniels and Smithies[46] for the mean span of a 1D random walk. We convert these equations to evaluate the mean span in 3D by dividing by $\sqrt{3}$ as

$$X = \begin{cases} \dfrac{1}{\sqrt{3}} \dfrac{2\mathcal{N}+1}{2^{\mathcal{N}}} \dfrac{\mathcal{N}!}{\left(\frac{\mathcal{N}}{2}\right)!\left(\frac{\mathcal{N}}{2}\right)!} - 1 \ (\mathcal{N} \text{ even}), \\ \dfrac{1}{\sqrt{3}} \dfrac{2\mathcal{N}+2}{2^{\mathcal{N}}} \dfrac{\mathcal{N}!}{\left(\frac{\mathcal{N}}{2}-\frac{1}{2}\right)!\left(\frac{\mathcal{N}}{2}+\frac{1}{2}\right)!} - 1 \ (\mathcal{N} \text{ odd}), \end{cases} \tag{13}$$

where $\mathcal{N}$ is the normalized contour length L/b. In Fig. 3, we observe that the fractional extension of IFJCs parallel to the channel axis is independent of the channel size and is unperturbed by confinement in the channel. However, the prediction of Eq. 13 for the mean span in 3D for $L/b \approx 1$ is not accurate as the prefactor $\sqrt{3}$ is valid only when $L \gg b$. Nonetheless, the collapse of the extension data for all channels gives further credence to the absence of discretization artifacts in these simulations.

Although the extension parallel to the channel is unchanged, there is an entropic penalty to squeeze the chain into the channel, and hence the confined chain has a higher free energy than the chain in the bulk. The change in free energy due to confinement in a channel for a FJC with $D \gg b$ and $L > b$ can be approximated as[49]

$$\begin{aligned} \beta\Delta F &= -\ln\left[\frac{P_{1D}^{\text{conf}}(N, \mathbf{R}_x)P_{1D}^{\text{conf}}(N, \mathbf{R}_y)P_{1D}^{\text{conf}}(N, \mathbf{R}_z)}{P_{1D}^{\text{free}}(N, \mathbf{R}_x)P_{1D}^{\text{free}}(N, \mathbf{R}_y)P_{1D}^{\text{free}}(N, \mathbf{R}_z)}\right] \\ &= -\ln\left(\frac{P_{1D}^{\text{conf}}(N, \mathbf{R}_y)}{P_{1D}^{\text{free}}(N, \mathbf{R}_y)}\right) - \ln\left(\frac{P_{1D}^{\text{conf}}(N, \mathbf{R}_z)}{P_{1D}^{\text{free}}(N, \mathbf{R}_z)}\right). \end{aligned} \tag{14}$$

It is evident from Eq. 14 that the free energy of confinement arises due to constraints imposed

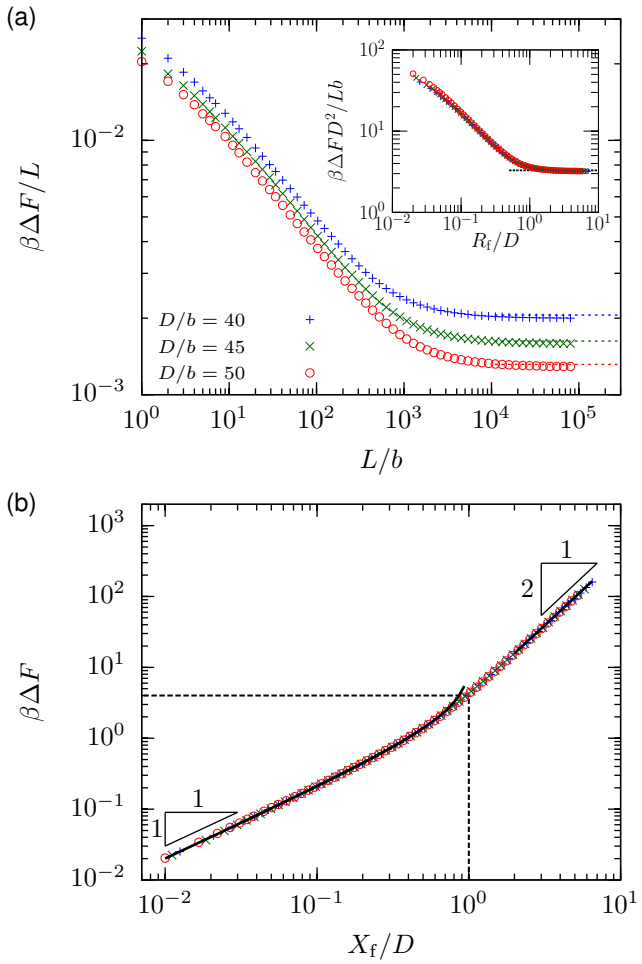

FIG. 4. (a) Free energy of ideal FJCs in 3 square channels of different sizes. The free energy values asymptote to the value given by Eq. 15 (dashed lines).[19,48]. In the inset, the free energy values are shown to reach asymptotic scaling for all 3 channels when $R_f \approx D$. The dashed line signifies the theoretically expected limit, $\pi^2/3$. (b) Free energy data for the 3 channels fall on a universal curve as per scaling theory, with an asymptotic scaling $\Delta F \sim (X_f/D)^2$ for $X_f \gg D$. The dashed lines show that the free energy of confinement is approximately $4k_BT$ for $X_f/D = 1$. The solid black lines show theoretical predictions: Eq. 17 for $X_f/D \lesssim 1$[49,50] and Eq. 15 for $X_f/D \gtrsim 1$. A scaling of $\Delta F \sim (X_f/D)^1$ is also seen for $X_f \ll D$.

in the y and z directions by the walls of the channel. Figure 4(a) shows the free energy of a confined IFJC for various channel sizes as a function of contour length L. Unlike extension, the free energy of confinement in different channels are never equal. Even at extremely small contour lengths (order of a few beads), the free energy values are unequal in different channels because of a different degree of entropy loss. However, in the long-chain limit, $\Delta F/L$ asymptotes to a constant value[35] and this asymptotic value when $L \gg D \gg b$ is

given by[19,48]

$$\beta\Delta F = \frac{\pi^2 Lb}{3D^2}. \tag{15}$$

Our simulation results in Fig. 4 show excellent agreement with this prediction.

Furthermore, akin to de Gennes' scaling theory for flexible real chains,[1,3,51] a scaling equation of the form

$$\beta\Delta F = \phi_{\Delta F}\left(\frac{R_\mathrm{f}}{D}\right) \tag{16}$$

can be written, where R_f is the root mean square end-to-distance in free solution and $\phi_{\Delta F}$ is a function such that $\phi_{\Delta F}(x) \sim x^2$ as $x \to \infty$ in the limit $R_\mathrm{f} \gg D \gg b$.[49] However, Eq. 16 does not hold if $R_\mathrm{f} \ll D$. Fortunately, in the limit $R_\mathrm{f} \ll D$ or more precisely $X_\mathrm{f} \ll D$, the confinement free energy in a channel is given by

$$\beta\Delta F = -\ln\left(1 - \frac{X_\mathrm{f}}{D}\right)^2, \tag{17}$$

where X_f is the mean span in free solution.[49,50] Now, the confinement free energy can be written as a similar function of the mean span in free solution as

$$\beta\Delta F = \Phi_{\Delta F}\left(\frac{X_\mathrm{f}}{D}\right). \tag{18}$$

Since the ratio $X_\mathrm{f}/R_\mathrm{f}$ is a constant for $R_\mathrm{f}, X_\mathrm{f} \gg b$, i.e $X_\mathrm{f}/R_\mathrm{f} \to \sqrt{8/3\pi}$,[46] $\Phi_{\Delta F}(x)$ has the following properties:

$$\Phi(x) : \begin{cases} = -\ln(1-x^2) & \text{if } x \ll 1, \\ \sim x^2 & \text{if } x \gg 1. \end{cases} \tag{19}$$

To verify Eq. 19, we plot the confinement free energy against X_f/D for 3 channel sizes as shown in Fig. 4(b). We observe that the free energy values for the three channels considered all fall on the same curve irrespective of the contour length.

Plotting free energy as a function of X_f/D also provides us with a way to identify cut-offs for the onset of asymptotic scaling. We find two distinct regimes in Fig. 4(b): (i) a weak confinement regime, where the bulk size of the chain is less than that of the channel width, and (ii) a strong confinement regime, where the average size of the chain in the bulk is greater than D. In the former, our free energy calculations agree with Eq. 17. Moreover, our data in Fig. 4(b) clearly show a distinct scaling of $\beta\Delta F \sim X_\mathrm{f}/D$ in the weak confinement

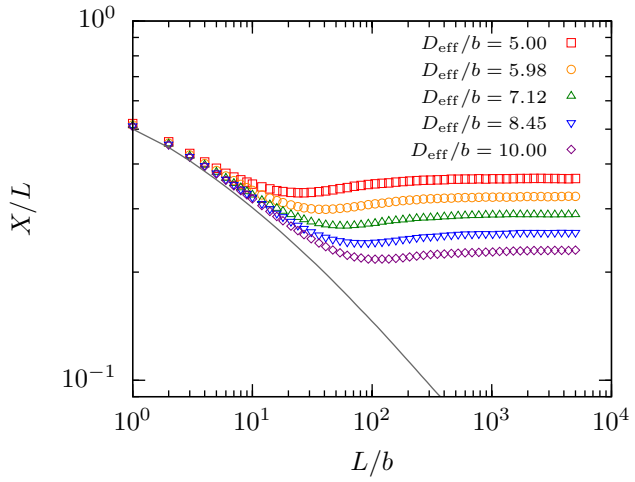

FIG. 5. Fractional extension of RFJCs ($a = w = b$) confined in channels with same $D_{\rm eff}$ values as in Fig. 3. The gray line corresponds to simulation results of a RFJC in free solution.

regime, because $\beta\Delta F = -\ln(1 - X_{\rm f}/D)^2 \approx 2X_{\rm f}/D$ if $X_{\rm f} \ll D$.

In the strong confinement regime ($X_{\rm f} > D$), the free energy values exhibit asymptotic scaling for $X_{\rm f}/D \gtrsim 1$, endorsing the fact the free energy attains limiting scaling when the chain as a whole feels the effect of confinement. Figure 4(b) also shows that $\Delta F \approx 4k_{\rm B}T$ when $X_{\rm f} = D$ thus supporting the widely prevalent notion that the confinement free energy is $\mathcal{O}(k_{\rm B}T)$ for a chain of unconfined size D.

2. Real freely jointed chains (RFJC)

In the presence of repulsive excluded volume interactions, confined flexible chains follow statistics outlined by Daoud and de Gennes in their seminal paper.[3] De Gennes[1] proposed that for a chain confined in a cylinder of diameter $D_{\rm cyl}$, in the long chain limit ($L \gg D_{\rm cyl}$), "the chain behaves as a sequence of blobs of diameter $D_{\rm cyl}$ which act as hard spheres and pack into a regular one-dimensional array."[1] A similar depiction of the chain as a 1D self-avoiding walk of blobs in square confinement leads to a predicted scaling, $X \sim L$. Figure 5 shows fractional extension of RFJCs confined in square channels with the same $D_{\rm eff}$ values as in Fig. 3. We observe that at very small chain lengths, the extension of the chain is the same as in free solution. However, as the chain length increases, the chain begins to backfold because of collisions with the walls. In contrast to the IFJC, the increase in backfolding induces self-repulsion, resulting in a rapid increase in the extension. Once the

average monomer concentration attains a threshold value, backfolding at the length scale of the channel size D is no longer possible due to self-avoidance.[12,28,31] This leads to a linear ordering of segments of the chain resulting in a linear scaling, $X \sim L$.

Analogous to the case of ideal flexible chains, the properties of real flexible chains in confinement have been studied with the use of diffusion-annihilation equations.[47,52] However, because of the difficulty in determining the annihilation term, a mean-field approximation is employed to account for the excluded volume interactions by means of self-consistent field theory.[47] Werner *et al.* recently showed that mean-field approximation does not yield satisfactory results as it neglects intrachain correlations, which are especially critical in determining properties of self-avoiding chains in confinement.[47]

Nonetheless, scaling theory can still be applied to interpret the behavior of RFJCs in confinement. For $X_\mathrm{f} \gg D_\mathrm{eff} \gg b$, the extension parallel to the axis of a channel was written by de Gennes in a scaling form as[1,3,53]

$$\frac{X}{X_\mathrm{f}} = \Phi_X \left(\frac{X_\mathrm{f}}{D_\mathrm{eff}} \right), \tag{20}$$

where X is the extension (mean span) in confinement, and X_f is the mean span in free solution. Similarly, a relation analogous to Eq. 18 for confinement free energy ΔF is[1,3]

$$\beta \Delta F = \Phi_{\Delta F} \left(\frac{X_\mathrm{f}}{D_\mathrm{eff}} \right), \tag{21}$$

where the functions Φ are defined such that $\Phi_X(x) \sim x^{1/\nu_\mathrm{F}-1}$ and $\Phi_{\Delta F}(x) \sim x^{1/\nu_\mathrm{F}}$ for $x \gg 1$ in accordance with the scaling laws in the de Gennes regime. Here, $\nu_\mathrm{F} \simeq 0.5877$ is the Flory exponent.[54,55] Also, recall from Sec. II A that $D_\mathrm{eff} = D - w$ is the effective width of the channel accessible to the centerline of the backbone of the polymer molecule. Note that for $x \ll 1$, $\Phi_{\Delta F}(x) = (1-x)^2$, wherein the quantity D in Eq. 17 has been replaced by D_eff. Agreement with Eqs. 20 and 21 is indicated by the collapse of the X/X_f curves in Fig. 6(a) and the $\beta \Delta F$ curves in Fig. 6(b) respectively.

Furthermore, we observe in Fig. 6(a) that confined RFJCs behave virtually like unconfined chains until the unconfined chain size X_f is approximately equal to the channel size D_eff. In other words, $X \approx X_\mathrm{f}$ for $X_\mathrm{f} \lesssim D_\mathrm{eff}$. Beyond this threshold value, i.e. when $X_\mathrm{f} \gtrsim D_\mathrm{eff}$, there is a sharp increase in the extension of the confined chain culminating in a scaling of

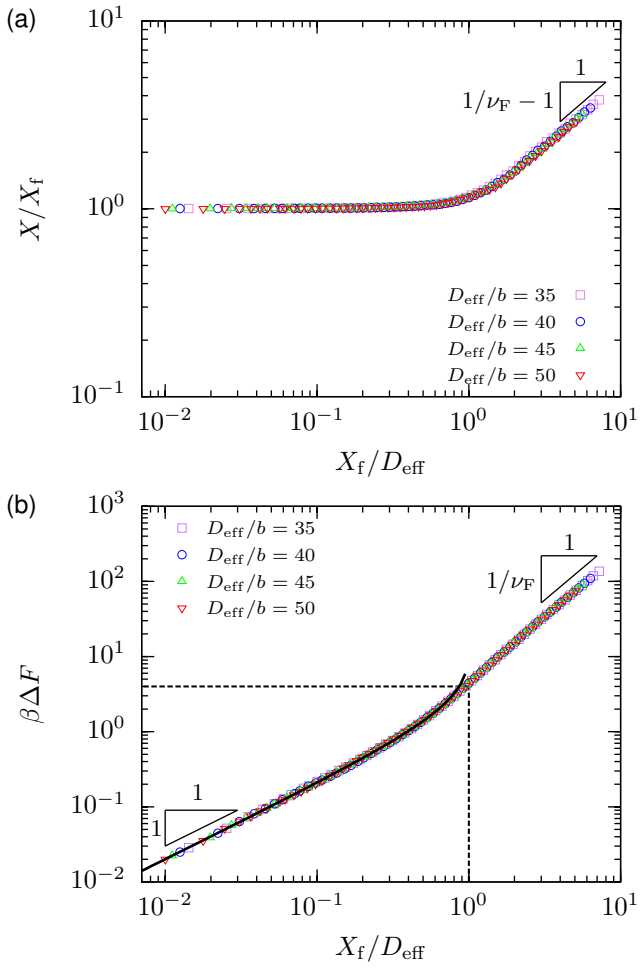

FIG. 6. (a) Ratio of extension in confinement with extension in the bulk versus ratio of the free-solution mean span with the channel size for 4 channels. (b) Confinement free energy for the chains under the same conditions. The dashed lines show that the confinement free energy is $\mathcal{O}(k_\mathrm{B}T)$ when $X_\mathrm{f}/D_\mathrm{eff} = 1$. The prediction in Eq. 22 is shown as a solid black line. Also shown is the scaling, $\beta\Delta F \sim X_\mathrm{f}/D_\mathrm{eff}$, in the weak confinement regime. Notice the scaling of both properties in the long-chain limit: $X/X_\mathrm{f} \sim (X_\mathrm{f}/D_\mathrm{eff})^{1/\nu_\mathrm{F}-1}$, and $\Delta F \sim (X_\mathrm{f}/D_\mathrm{eff})^{1/\nu_\mathrm{F}}$. The data shown here corresponds to RFJCs of contour length L ranging from $L = b$ to $L = 5000b$.

$X/X_\mathrm{f} \sim (X_\mathrm{f}/D_\mathrm{eff})^{1/\nu_\mathrm{F}-1}$.

The confinement free energy also exhibits two distinct regimes as shown in Fig. 6(b). We find that free energy in the weak confinement regime ($X_\mathrm{f} \lesssim D_\mathrm{eff}$) agrees well with the following relation, which is essentially a restatement of Eq. 17:

$$\beta\Delta F = -\ln\left(1 - X_\mathrm{f}/D_\mathrm{eff}\right)^2. \tag{22}$$

We also note that the slope of the ΔF curve abruptly changes when $X_\mathrm{f}/D_\mathrm{eff} \approx 1$ to a

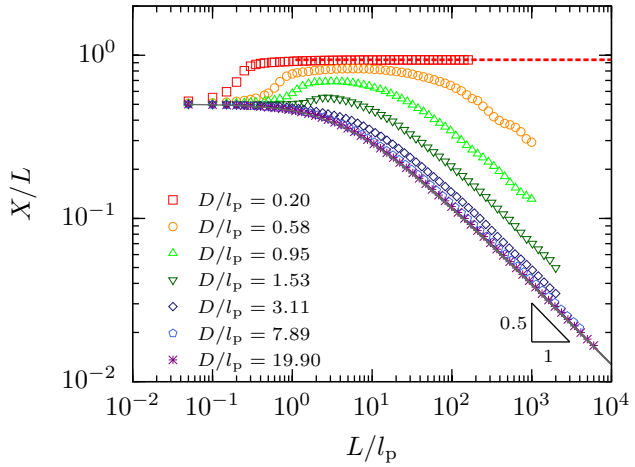

FIG. 7. Fractional extension of IWLCs with $l_p/a = 20$ versus contour length for various channel sizes. The gray line shows simulation results for fractional extension of the chain in free solution with an expected slope of -0.5 in the long-chain limit. The red dashed line corresponds to the prediction in the Odijk regime given by Eq. 23.[57]

slope $1/\nu_F$ as predicted by Daoud and de Gennes,[3] indicating that the statistics of confined RFJCs transition quickly to the long-chain limit once the chain size is large enough to form a blob of size D_{eff}. A careful examination of Fig. 6(b) shows that $\Delta F \approx 4k_BT$ for $X_f \approx D_{eff}$, which is in agreement with previous predictions that the confinement free energy of a blob is $\mathcal{O}(k_BT)$.[1,3,12,56]

3. Ideal wormlike chains (IWLC)

In the seminal paper on properties of confined stiff polymers in extreme confinement, Odijk introduced a new length scale, $\lambda \simeq D^{2/3}l_p^{1/3}$, that corresponds to the length of a deflection segment.[4] According to Odijk's theory, the extension of IWLCs with $L \gg \lambda$ in a square channel of size D can be written as

$$X = L\left[1 - \alpha_{\square}\left(\frac{D}{l_p}\right)^{2/3}\right], \tag{23}$$

when $D \ll l_p$. The prefactor has been calculated by Yang, Burkhardt, and Gompper[57] as $\alpha_{\square} = 0.18274$. Equation 23 shows that the scaling of the extension, $X \sim L$, is markedly different for IWLCs in comparison to IFJCs, where $X \sim L^{0.5}$ in the long-chain limit. Moreover, the extension of IFJCs is equal to the bulk value and therefore does not depend on D,

unlike the extension of IWLCs in the Odijk regime. Furthermore, little is known about the behavior of IWLCs when $l_p \gtrsim D$, as most studies with WLCs involve chains with excluded volume.[13,16,17,58] Here, we study the extension behavior of IWLCs in confinement as a function of channel size and contour length, in the interest of demarcating the effect of stiffness on the properties of confined semiflexible polymers.

The fractional extension of stiff ideal chains confined in channels of various sizes is shown in Fig. 7. We note here that unlike the figures in Secs. III A 1 and III A 2, we plot our data with the contour length normalized with the persistence length, l_p, as is the norm for wormlike chains. For all the channels, we observe that X/L starts at 0.5, which is the value of the fractional extension in the bulk for a rod given by

$$\frac{X}{L} = \frac{\int_0^\pi |\cos\theta| \sin\theta \mathrm{d}\theta}{\int_0^\pi \sin\theta \mathrm{d}\theta} = 0.5, \tag{24}$$

where θ is the polar angle with the x axis.[59] At these values of the contour length L, the chain is almost unaffected by confinement and has virtually the same rotational freedom as in free solution. For $D \lesssim l_p$, as the chain length increases, the chain begins to feel the walls and aligns with the axis of the channel. This is reflected in Fig. 7 as a rise in the fractional extension from the bulk value, at short chain lengths. For $D/l_p = 0.20$, the fractional extension is practically at the asymptotic value when L/l_p is approximately 0.5. At this value of L, the number of deflection segments ($\lambda \approx l_p^{1/3} D^{2/3}$) is approximately $L/(l_p^{1/3} D^{2/3}) \approx 1.5$, even though the chain is smaller than a single persistence length. This implies that the transition to asymptotic Odijk extension is rather quick, i.e. a chain that can form a few deflection segments is sufficiently long to exhibit behavior as in Eq. 23.

For $D/l_p = 0.58$ and 0.95, we observe significant stretching in the unconfined direction, i.e. $X/X_f > 1$, as shown in Fig. 7. Particularly in the case of $D/l_p = 0.58$, the chain seems to follow Odijk-like $X \sim L$ behavior till about $L/l_p = 10$. However, after the chain reaches a certain length, which Odijk terms the global persistence length,[10] the entropic constraints of the walls are not strong enough to prevent formation of hairpins. Formation of hairpins by ideal chains leads to an extension X that is not linear in the contour length.[11,16] As the channel size increases, the amount of backfolding of these IWLCs increases, leading to decreasing fractional extension X/L with L. We note here that the noise in the data shown in Fig. 7 at high L for intermediate channel sizes is due to high fluctuations of extension in

this region of confinement. Similar behavior has been observed before, both in simulations[60] and experiments.[2,8]

The fluctuations in the extension decrease as the channel size gets much bigger than the persistence length. When $D/l_p = 19.90$, the fractional extension of the chain is indistinguishable from the free solution curve, indicating stiffness has very little effect on stretching of the chain in this regime. In other words, the chain behaves exactly like an IFJC confined in a wide channel. For channel sizes such as $D/l_p = 3.11$ and $D/l_p = 7.89$, however, we observe that the fractional extension is almost identical to that of a chain in bulk, though there is moderate stretching.

Confinement free energy of channel-confined IWLCs as a function of channel size has been studied by our group previously.[19] It was found that the confinement free energy transitions from $\Delta F_{conf} \sim D^{-2/3}$ in the Odijk regime to $\Delta F_{conf} \sim D^{-2}$ in weak confinement,[19] in agreement with free energy calculations of IWLCs confined in slits.[48] In addition, these results are also in qualitative agreement with recent work on confinement free energy of IWLCs in channels.[61] This D^{-2} scaling of the free energy is analogous to the case of confined IFJCs shown in Sec.III A 1, again reinforcing the fact that confined IWLCs show the same properties of equivalent IFJCs in weak confinement.

In summary, extension of IWLCs transitions from the Odijk regime in extreme confinement ($D \ll l_p$) to the behavior of unconfined IWLCs in weak confinement ($D \gg l_p$). We term this regime of weak confinement the "bulk-like" regime for IWLCs, as the extension is given by the bulk extension, just as in the case of confined IFJCs. It is interesting to note that our results also indicate the presence of a broad transition regime ($0.5 \lesssim D/l_p \lesssim 20$) between the Odijk regime and the bulk-like regime.

B. Real wormlike chains (RWLC)

1. Theoretical aspects

We now turn our attention to the case of RWLCs, which exhibit a nontrivial combination of the properties of RFJCs and IWLCs shown in Secs. III A 2 and III A 3 respectively. When $D \ll l_p$, the chain is in the Odijk regime where the properties are dominated by chain stiffness. In contrast, when $D \gg l_p$ and $L \gg D$, we recover the de Gennes regime, which is

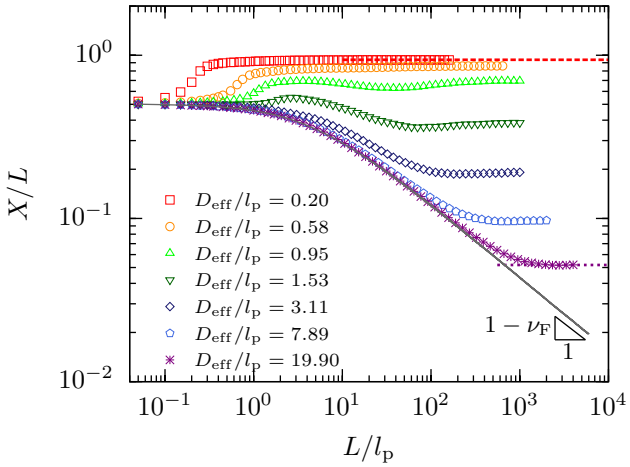

FIG. 8. Fractional extension of RWLCs with $l_p/a = 20$ versus contour length for the same D_{eff} values as in Fig. 7. The gray line depicts the fractional extension for the chain in free solution with an expected slope of $-(1 - \nu_F) \simeq -0.42$ in the long-chain limit. Our results agree with predicted extension in the Odijk regime (red dashed line)[57] and prior results for the long-chain limit in the de Gennes regime (purple dotted line).[19] However, most other curves fall in the transition regime.

governed by excluded volume. However, in the region $D \approx l_p$, there are two contributing effects leading to stretching in the unconfined direction, namely stiffness and excluded volume. This complicated interplay between stiffness and excluded volume is not well understood, and hence there is little consensus about the mechanism of stretching in this transition region.

Here, we seek to gain further understanding of the mechanism of stretching in confinement by examining the effect of contour length on the extension. Figure 8 shows the fractional extension of real wormlike chains (RWLCs) for the same D_{eff}/l_p values as in Fig. 7. For $D_{eff}/l_p = 0.20$, the curve is identical to the case of an IWLC hinting that excluded volume does not have any effect on stretching of the chain in the Odijk regime. For bigger channels considered in Sec. III A 3, recall that we did not observe the scaling $X \sim L$, presumably due to long-range backfolding of the chain. In contrast, RWLCs reach an asymptotic value of the fractional extension in the long-chain limit, regardless of the channel size. For instance, in the case of $D_{eff}/l_p = 0.58$, the IWLC shows a drop in the fractional extension around $L/l_p = 20$ as shown in Fig. 7. This descent of X/L is absent in Fig. 8, showing that backfolding is minimal for RWLCs at this channel size. This stark contrast between extension behavior of IWLCs and RWLCs demonstrates that excluded volume between distal segments suppresses

backfolding of confined semiflexible chains.

For larger channels such as the one with size $D_{\rm eff}/l_{\rm p} = 1.53$, the drop in X/L around $L/l_{\rm p} = 10$ in Fig. 8 signifies backfolding. However, as the chain length increases, this backfolding in turn leads to an amplification of excluded volume interactions. Accordingly, the curve plateaus to an asymptotic fractional extension with increasing chain length, showing a linear scaling in the contour length, $X \sim L$.

For the biggest channel, i.e. when $D_{\rm eff}/l_{\rm p} = 19.90$, we observe that the chain follows the free solution curve up to about $L/l_{\rm p} = 100$, which is reminiscent of the behavior of IWLCs in weak confinement. However, self-avoidance induced by backfolding eventually causes the chain to swell in the direction parallel to the axis of the channel. Thereafter, the X/L curve in Fig. 8 branches off from the free-solution curve, plateauing to the value previously observed in the de Gennes regime.[19] The resulting constant fractional extension is a consequence of the cigar-like conformation formed by the chain in this regime.[1]

2. DNA in nanochannels and other practical implications

Following the seminal experiments by Reisner *et al.*,[8] there has been tremendous interest in understanding the static and dynamic properties of nanochannel-confined wormlike chains, particularly DNA.[10,11,16–19,58,62–64] In addition, nascent genome mapping technologies such as DNA barcoding in nanochannels are based on the assumption that there is a one-to-one linear relationship between the separation of markers in the channel and the genomic length between two points on a DNA molecule.[2,7,65] We know from results reported in the preceding sections that the linear scaling, $X \sim L$, for RWLCs in confinement is valid when the chain is long enough to contain several statistical segments such as deflection segments or blobs, depending on the regime of confinement. One of the aspects that is often overlooked is whether the data obtained from the aforementioned experiments and simulations satisfies conditions for the asymptotic linear scaling, $X \sim L$, in channel confinement.

We recently showed that the onset of asymptotic scaling, $X \sim L^{\nu_{\rm F}}$, for unconfined DNA in a high ionic strength buffer occurs at a molecular weight of approximately 1 Mbp.[26] One of the consequences of this outcome is that λ-DNA, the experimental workhorse, lies well within the transition regime connecting $\nu_{\rm id} = 0.5$, for an ideal coil and $\nu_{\rm F} = 0.5877$, the universal exponent for swollen coils in free solution. It is unclear how these molecular-weight

dependent results for chains in the bulk reconcile with those in quasi-1D square confinement as in a nanochannel. To resolve such uncertainties, we examine the finite length effects of DNA in nanochannels to establish limits for the validity of the linear scaling of the extension, $X \sim L$.

In order to simulate DNA in nanochannels, it is important to choose the appropriate set of parameters that account for the interactions present in an experimental system. As in our previous work,[17,19,26] we use parameters for DNA in a high ionic strength (165 mM) buffer, 5×TBE, in which electrostatic interactions are highly screened. Such a value of the ionic strength allows us to use a hard-core repulsion for the excluded volume potential as a good approximation. Further, the value of the persistence length at high ionic strength is less ambiguous, as there exist discrepancies for the value of l_p at low ionic strengths.[26,66,67] Consequently, we use an effective width of $w = 4.6\,\mathrm{nm}$ from Stigter's theory[68] and a persistence length of $l_\mathrm{p} = 53\,\mathrm{nm}$[66,69] corresponding to the aforementioned ionic strength. Accordingly, the contour length of DNA in units of base pairs (bp) is obtained from Nw/l_bp, where $l_\mathrm{bp} = 0.34\,\mathrm{nm}$ is the rise per base pair in DNA.

In our recent work, simulations employing these parameters yielded good agreement with experimental scattering data for the radius of gyration of unconfined DNA.[26] Notwithstanding this agreement, our simulation results did not conform with single molecule fluorescence microscopy data.[26] We believe that this discrepancy may be due to the presence of intercalating dyes in these experiments. These dyes alter the size of DNA by changing the contour length (L),[70–73] and conceivably even properties such as the width (w) and the persistence length (l_p).[71] There is also contrary evidence suggesting that the persistence length more or less remains constant and is independent of the amount of bound YOYO-1.[73] Additionally, the dependence of w on the dye concentration is still unclear. This makes direct comparison of simulations with experiments difficult, as most experiments with DNA in nanochannels employ dyed DNA. Moreover, the effect of electrostatics on the wall-DNA interaction is still unclear,[2,17] and this further complicates modeling of DNA in a nanochannel. Our simulations thus make the simplifying assumption that the depletion width due to electrostatic interactions between the wall and DNA is $w/2$. In view of the confusion surrounding the right parameters for dyed DNA, we stick to the parameters for undyed, "naked" DNA listed in the previous paragraph.

Figure 9 displays results for extension of undyed DNA calculated using two metrics: (i)

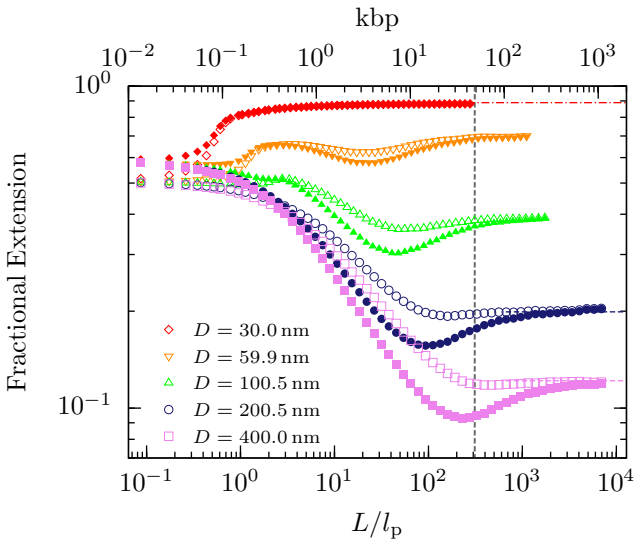

FIG. 9. Mean span X (unfilled symbols) and projection of the end-to-end distance on the axis of the channel R_x (filled symbols) normalized by the contour length for confined, undyed DNA in a high ionic strength buffer. Note that the x axis at the bottom indicates the number of persistence lengths of the chain and the x axis at the top denotes the length of DNA in units of kilobase pairs. The red dashed-dotted line corresponds to the asymptotic fractional extension in the Odijk regime.[57]. The dashed lines corresponding to the two biggest channels show the empirical fit obtained by Tree, Wang, and Dorfman [19] for the long-chain limit in the de Gennes regime. The molecular weight of λ-DNA is shown as a vertical gray dashed line.

the mean span (X); and (ii) x-projection of the end-to-end distance (R_x). As expected, we see a trend similar to Fig. 8. Among the two metrics shown, the span (X), which is the common experimental measure,[8,9,17,74] is less sensitive to backfolding compared to the end-to-end distance projection (R_x) on the channel axis. Unsurprisingly, in the Odijk regime, X and R_x are almost identical except at very short lengths of the chain ($L < O(\lambda)$) due to the absence of backfolding. In contrast, for the large channels, we observe that X and R_x asymptotically approach a limiting value which in turn agrees with the predicted extension in the de Gennes regime, independent of the metric used to describe the extension.[19]

An interesting feature of Fig. 9 is that X and R_x are equal in the long chain limit irrespective of the confinement regime. This result is a testament to the notion of linear ordering of blobs for self-avoiding chains in quasi-1D confinement, outside the Odijk regime. Correspondingly, the apparent confusion surrounding the earliest reports of simulations on DNA extension suggesting that $X \not\sim L$ seems be an effect of finite chain length as the longest chain used in that work was 14.8 kbp long.[13] Figure 9 also furnishes us with a convenient rubric to check if a chain is sufficiently long to be in the asymptotic region of the blob regime

in which $X \sim L$ applies. This is especially important for conventional Metropolis Monte Carlo simulations, where each simulation gathers data for a single chain length. In order to ascertain whether the chain is long enough to be in the asymptotic region, one might have to perform multiple simulations at various lengths and verify that the properties fall on a universal curve. A relatively simple and convenient way to ensure the validity of asymptotic behavior ($X \sim L$) is to calculate X and R_x from the same simulation, and check if the two quantities are the same within the margin of error.

It is customary to presume that the span measured from fluorescence microscopy experiments is the same as the end-to-distance, which itself is based on the assumption that the chain has reached the asymptotic limit.[2,8,74] However, our findings suggest that X and R_x are not necessarily equal for λ-DNA, as there is a gradual deviation of R_x from X with increase in channel size. We find from Fig. 9 that the relative error in fractional extension for λ-DNA from the asymptotic value is less than 3% for the channel sizes considered here, given that it is calculated from the mean span. In contrast, the error is as high as 20% for the largest channel, if the fractional extension is calculated from the x-projection of the end-to-end distance. This difference in the relative error of the fractional extension obtained from the two metrics is apparent when the data is plotted with a logarithmic axis as shown in Fig. 9. These results demonstrate that although λ-DNA is not truly in the asymptotic limit, the fractional extension measured from the span is within 3% of the asymptotic value for channel sizes typically used in experiments.

Furthermore, the w/l_p ratio increases with decreasing ionic strength for DNA, indicating that the excluded volume becomes increasingly more important at low ionic strengths.[26] As most experiments are performed at ionic strengths lower than the one used in our simulations,[8,9,74] we expect excluded volume to have a stronger effect on extension data obtained from experiments. This implies that the onset of asymptotic scaling, $X \sim L$, occurs for chains with lower L compared to the ones dealt in our work. Therefore, we conclude that if the fractional extension is inferred from the measurement of the span, chains of the contour length of λ-DNA or above yield nearly asymptotic results for X/L.

IV. Concluding remarks

By independently controlling the effects of excluded volume and stiffness, we studied the equilibrium properties of single polymer chains in channel confinement. Through our large scale PERM simulations, we verified that confinement does not have any effect on the extension of ideal freely jointed chains, provided that the confinement size is not comparable to the Kuhn length. Further, our extension and free energy calculations for self-avoiding flexible chains agree well with de Gennes' theory. We also demonstrated that as the confinement width increases, the extension of ideal stiff chains exhibits a broad transition regime between the Odijk regime and a stretch-free bulk-like regime.

For self-avoiding stiff chains, we confirmed that the extension is linear in the contour length in the long-chain limit regardless of the regime of confinement, albeit due to different underlying mechanisms. In the Odijk regime, this is due to the linear ordering of deflection segments whereas outside the Odijk regime the arrangement of nearly non-interpenetrating blobs in a channel leads to this linear scaling. The onset of this asymptotic scaling in extension in the Odijk and the de Gennes regimes correspond to the chain length at which the chain contains a few deflection segments or de Gennes blobs, as the case may be. However, the behavior within the transition regime is a function of the interplay between stiffness and excluded volume.[11]

Irrespective of the degree of confinement the projection of the end-to-distance on the axis and the mean span parallel to the axis of the channel were found to be equal in the long-chain limit. Although the chain length of λ-DNA is not sufficient to exactly satisfy this condition for all the channel sizes considered here, we inferred that λ-DNA is long enough to exhibit nearly asymptotic value of the fractional extension. This is because the fractional extension measured from the mean span for λ-DNA in a high ionic strength buffer is within 3% of the asymptotic value for square channels of sizes as high as 400 nm. The systematic error in the fractional extension due to finite chain length of λ-DNA measured in experiments is therefore negligible especially considering various other kinds of errors introduced in quantities such as the exact geometry of the nanofabricated device, and the image processing required to extract the mean extension from fluorescence intensity data.

Our findings remind us to be wary of finite chain length artifacts as we study the physics of semiflexible polymers in confinement. Although long-range excluded volume effects are

suppressed by the walls of the channels,[26] one has to be cautious in interpreting results from simulations and experiments, especially when dealing with short chain lengths. Dynamic properties such as the diffusion coefficient,[63] and the relaxation time in confinement[60] are also affected by finite chain length.[26] Likewise, short length-scale effects arising from the semiflexible nature of DNA have been shown to affect diffusivity in both slit-confinement[75] and channel-confinement.[63] It remains to be seen how the progression to asymptotic scaling for dynamic properties is related to that of the static properties discussed here, keeping in mind that the transition to asymptotic scaling is slower for dynamic properties in the bulk.[76,77]

Acknowledgments

This work was supported by grants from the NIH (R01-HG006851), the NSF (CBET-1262286) and the David and Lucile Packard Foundation to KDD. DRT also acknowledges the support from a Doctoral Dissertation Fellowship by the University of Minnesota. Y. Wang thanks the National Natural Science Foundation of China (Grant No. 21204061) for their support. We thank Patrick S. Doyle (MIT) for providing a preprint of their recent work and the University of Minnesota Supercomputing Institute for providing computational resources for our simulations.

References

[1] P. G. de Gennes, *Scaling Concepts in Polymer Physics* (Cornell University Press, 1979).
[2] W. Reisner, J. N. Pedersen, and R. H. Austin, Rep. Prog. Phys. **75**, 106601 (2012).
[3] M. Daoud and P. G. de Gennes, J. Phys. France **38**, 85 (1977).
[4] T. Odijk, Macromolecules **16**, 1340 (1983).
[5] S. L. Levy and H. G. Craighead, Chem. Soc. Rev. **39**, 1133 (2010).
[6] F. Persson and J. O. Tegenfeldt, Chem. Soc. Rev. **39**, 985 (2010).
[7] K. D. Dorfman, S. B. King, D. W. Olson, J. D. P. Thomas, and D. R. Tree, Chem. Rev. **113**, 2584 (2013).
[8] W. Reisner, K. J. Morton, R. Riehn, Y. M. Wang, Z. Yu, M. Rosen, J. C. Sturm, S. Y. Chou, E. Frey, and R. H. Austin, Phys. Rev. Lett. **94**, 196101 (2005).
[9] W. Reisner, J. P. Beech, N. B. Larsen, H. Flyvbjerg, A. Kristensen, and J. O. Tegenfeldt, Phys. Rev. Lett. **99**, 058302 (2007).
[10] T. Odijk, J. Chem. Phys. **125**, 204904 (2006).
[11] T. Odijk, Phys. Rev. E **77**, 060901 (2008).
[12] C. Zhang, F. Zhang, J. A. van Kan, and J. R. C. van der Maarel, J. Chem. Phys. **128**, 225109 (2008).
[13] P. Cifra, Z. Benková, and T. Bleha, J. Phys. Chem. B **113**, 1843 (2009).

[14]F. Persson, P. Utko, W. Reisner, N. B. Larsen, and A. Kristensen, Nano Lett. **9**, 1382 (2009).
[15]P. Cifra, Z. Benková, and T. Bleha, Phys. Chem. Chem. Phys. **12**, 8934 (2010).
[16]P. Cifra and T. Bleha, Soft Matter **8**, 9022 (2012).
[17]Y. Wang, D. R. Tree, and K. D. Dorfman, Macromolecules **44**, 6594 (2011).
[18]T. Su, S. K. Das, M. Xiao, and P. K. Purohit, PLoS One **6**, e16890 (2011).
[19]D. R. Tree, Y. Wang, and K. D. Dorfman, Phys. Rev. Lett. **110**, 208103 (2013).
[20]L. Dai, S. Y. Ng, P. S. Doyle, and J. R. C. van der Maarel, ACS Macro Lett. **1**, 1046 (2012).
[21]E. Werner, F. Persson, F. Westerlund, J. O. Tegenfeldt, and B. Mehlig, Phys. Rev. E **86**, 041802 (2012).
[22]Z. Benková and P. Cifra, Macromolecules **45**, 2597 (2012).
[23]C. Bustamante, J. Marko, E. Siggia, and S. Smith, Science **265**, 1599 (1994).
[24]F. Brochard-Wyart, T. Tanaka, N. Borghi, and P.-G. de Gennes, Langmuir **21**, 4144 (2005).
[25]L. Dai and P. S. Doyle, Macromolecules **46**, 6336 (2013).
[26]D. R. Tree, A. Muralidhar, P. S. Doyle, and K. D. Dorfman, Macromolecules **46**, 8369 (2013).
[27]J. Wang and H. Gao, J. Chem. Phys. **123**, 084906 (2005).
[28]H.-P. Hsu and P. Grassberger, Eur. Phys. J. B **36**, 209 (2003).
[29]H.-P. Hsu and P. Grassberger, J. Chem. Phys. **120**, 2034 (2004).
[30]H.-P. Hsu and P. Grassberger, J. Stat. Phys. **144**, 597 (2011).
[31]H.-P. Hsu and K. Binder, Soft Matter **9**, 10512 (2013).
[32]J. Schellman, Biopolymers **13**, 217 (1974).
[33]M. Rubinstein and R. H. Colby, *Polymer Physics* (OUP Oxford, 2003).
[34]A. Grosberg and A. Khokhlov, *Statistical Physics of Macromolecules* (AIP, New York, 1994).
[35]M. Doi and S. Edwards, *The Theory of Polymer Dynamics* (Clarendon Press Oxford, 1986).
[36]P. Grassberger, Phys. Rev. E **56**, 3682 (1997).
[37]T. Prellberg and J. Krawczyk, Phys. Rev. Lett. **92**, 120602 (2004).
[38]K. Binder, ed., *Monte Carlo and Molecular Dynamics Simulations in Polymer Science* (Oxford University Press, 1995).
[39]D. Frenkel and B. Smit, *Understanding Molecular Simulation, Second Edition: From Algorithms to Applications (Computational Science)*, 2nd ed. (Academic Press, 2001).
[40]E. J. J. van Rensburg, J. Phys. A: Math. Theor. **42**, 323001 (2009).
[41]T. Prellberg, EPJ Web of Conferences **44**, 01001 (2013).
[42]M. P. Allen and D. J. Tildesley, *Computer Simulation of Liquids* (Oxford University Press, 1987).
[43]P. Grassberger and R. Hegger, J. Chem. Phys. **102**, 6881 (1995).
[44]N. Madras and A. D. Sokal, J. Stat. Phys. **50**, 109 (1988).
[45]G. H. Fredrickson, *The Equilibrium Theory of Inhomogeneous Polymers* (Clarendon Press Oxford, 2006).
[46]H. E. Daniels and F. Smithies, Math. Proc. Cambridge Philos. Soc. **37**, 244 (1941).
[47]E. Werner, F. Westerlund, J. O. Tegenfeldt, and B. Mehlig, Macromolecules **46**, 6644 (2013).
[48]J. Z. Y. Chen and D. E. Sullivan, Macromolecules **39**, 7769 (2006).
[49]A. A. Gorbunov and A. M. Skvortsov, Adv. Colloid Interface Sci. **62**, 31 (1995).
[50]Y. Wang, I. Teraoka, F. Y. Hansen, G. H. Peters, and O. Hassager, Macromolecules **43**, 1651 (2010).
[51]K. F. Freed, *Renormalization group theory of macromolecules* (Wiley New York et al., 1987).
[52]E. A. DiMarzio, J. Chem. Phys. **42**, 2101 (1965).
[53]P.-G. de Gennes, in *Polymers in Confined Environments*, Advances in Polymer Science, Vol. 138, edited by S. Granick, K. Binder, P.-G. Gennes, E. Giannelis, G. Grest, H. Hervet, R. Krishnamoorti, L. Léger, E. Manias, E. Raphaël, and S.-Q. Wang (Springer Berlin Heidelberg, 1999) pp. 91–105.
[54]B. Li, N. Madras, and A. Sokal, J. Stat. Phys. **80**, 661 (1995).
[55]N. Clisby, Phys. Rev. Lett. **104**, 055702 (2010).

[56]E. Raphael and P. Pincus, J. Phys. II France **2**, 1341 (1992).
[57]Y. Yang, T. W. Burkhardt, and G. Gompper, Phys. Rev. E **76**, 011804 (2007).
[58]P. Cifra, J. Chem. Phys. **131**, 224903 (2009).
[59]Y. Wang, G. H. Peters, F. Y. Hansen, and O. Hassager, J. Chem. Phys. **128**, 124904 (2008).
[60]D. R. Tree, Y. Wang, and K. D. Dorfman, Biomicrofluidics **7**, 054118 (2013).
[61]J. Z. Y. Chen, Macromolecules **46**, 9837 (2013).
[62]S. Köster, D. Steinhauser, and T. Pfohl, J. Phys.: Condens. Matter **17**, S4091 (2005).
[63]D. R. Tree, Y. Wang, and K. D. Dorfman, Phys. Rev. Lett. **108**, 228105 (2012).
[64]W. F. Reinhart, D. R. Tree, and K. D. Dorfman, Biomicrofluidics **7**, 024102 (2013).
[65]Y. Wang, W. F. Reinhart, D. R. Tree, and K. D. Dorfman, Biomicrofluidics **6**, 014101 (2012).
[66]A. V. Dobrynin, Macromolecules **39**, 9519 (2006).
[67]J. Skolnick and M. Fixman, Macromolecules **10**, 944 (1977).
[68]D. Stigter, Biopolymers **16**, 1435 (1977).
[69]C.-C. Hsieh, A. Balducci, and P. S. Doyle, Nano Lett. **8**, 1683 (2008).
[70]O. B. Bakajin, T. A. J. Duke, C. F. Chou, S. S. Chan, R. H. Austin, and E. C. Cox, Phys. Rev. Lett. **80**, 2737 (1998).
[71]L. Nyberg, F. Persson, B. Åkerman, and F. Westerlund, Nucleic Acids Res. **41**, e184 (2013).
[72]M. L. Bennink, O. D. Schärer, R. Kanaar, K. Sakata-Sogawa, J. M. Schins, J. S. Kanger, B. G. de Grooth, and J. Greve, Cytometry **36**, 200 (1999).
[73]K. Günther, M. Mertig, and R. Seidel, Nucleic Acids Res. **38**, 6526 (2010).
[74]J. O. Tegenfeldt, C. Prinz, H. Cao, S. Chou, W. W. Reisner, R. Riehn, Y. M. Wang, E. C. Cox, J. C. Sturm, P. Silberzan, and R. H. Austin, Proc. Natl. Acad. Sci. U.S.A. **101**, 10979 (2004).
[75]L. Dai, D. R. Tree, J. R. C. van der Maarel, K. D. Dorfman, and P. S. Doyle, Phys. Rev. Lett. **110**, 168105 (2013).
[76]M. L. Mansfield and J. F. Douglas, Macromolecules **41**, 5412 (2008).
[77]M. L. Mansfield and J. F. Douglas, Soft Matter **9**, 8914 (2013).

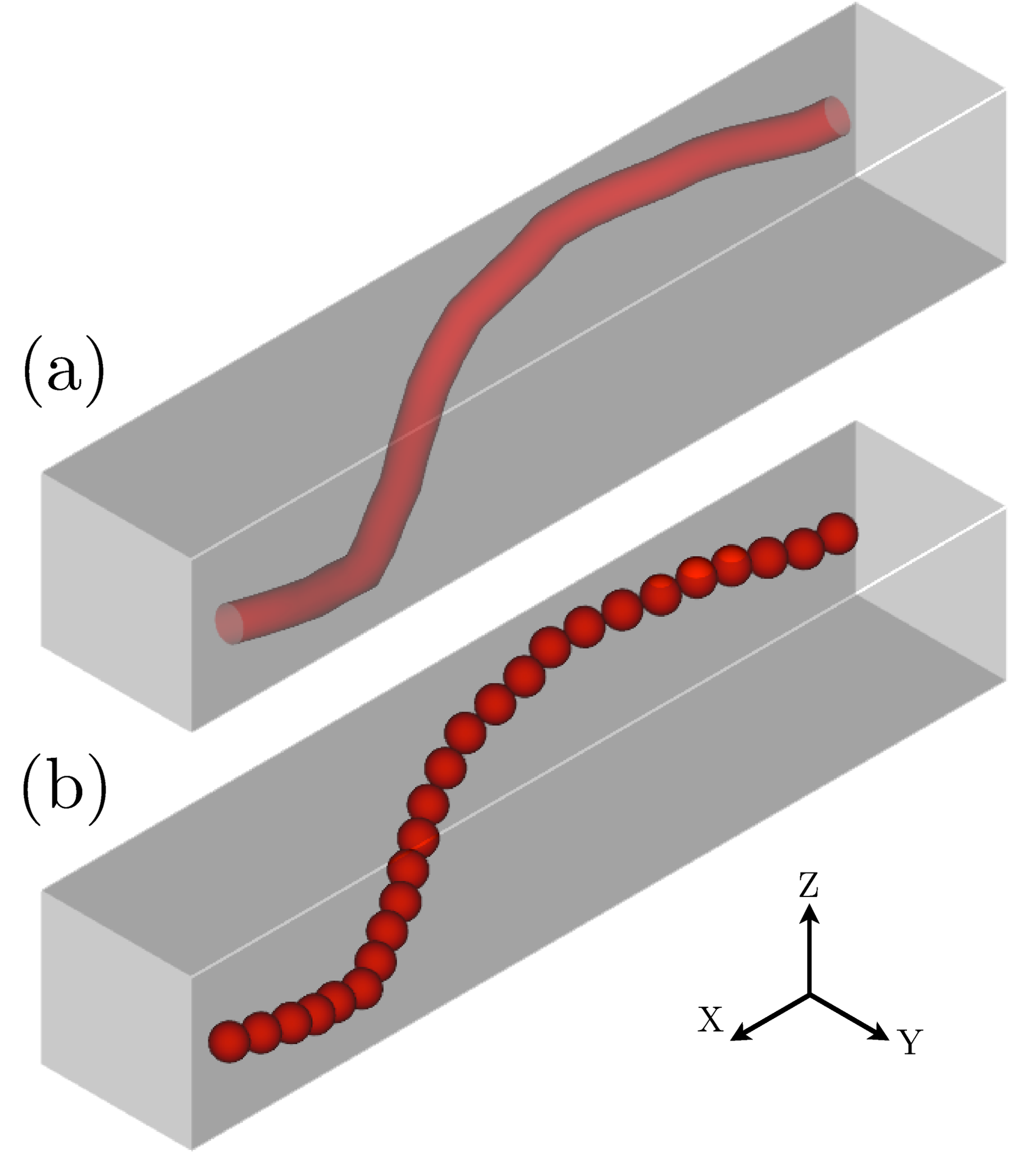
(a)
(b)
Z
X
Y

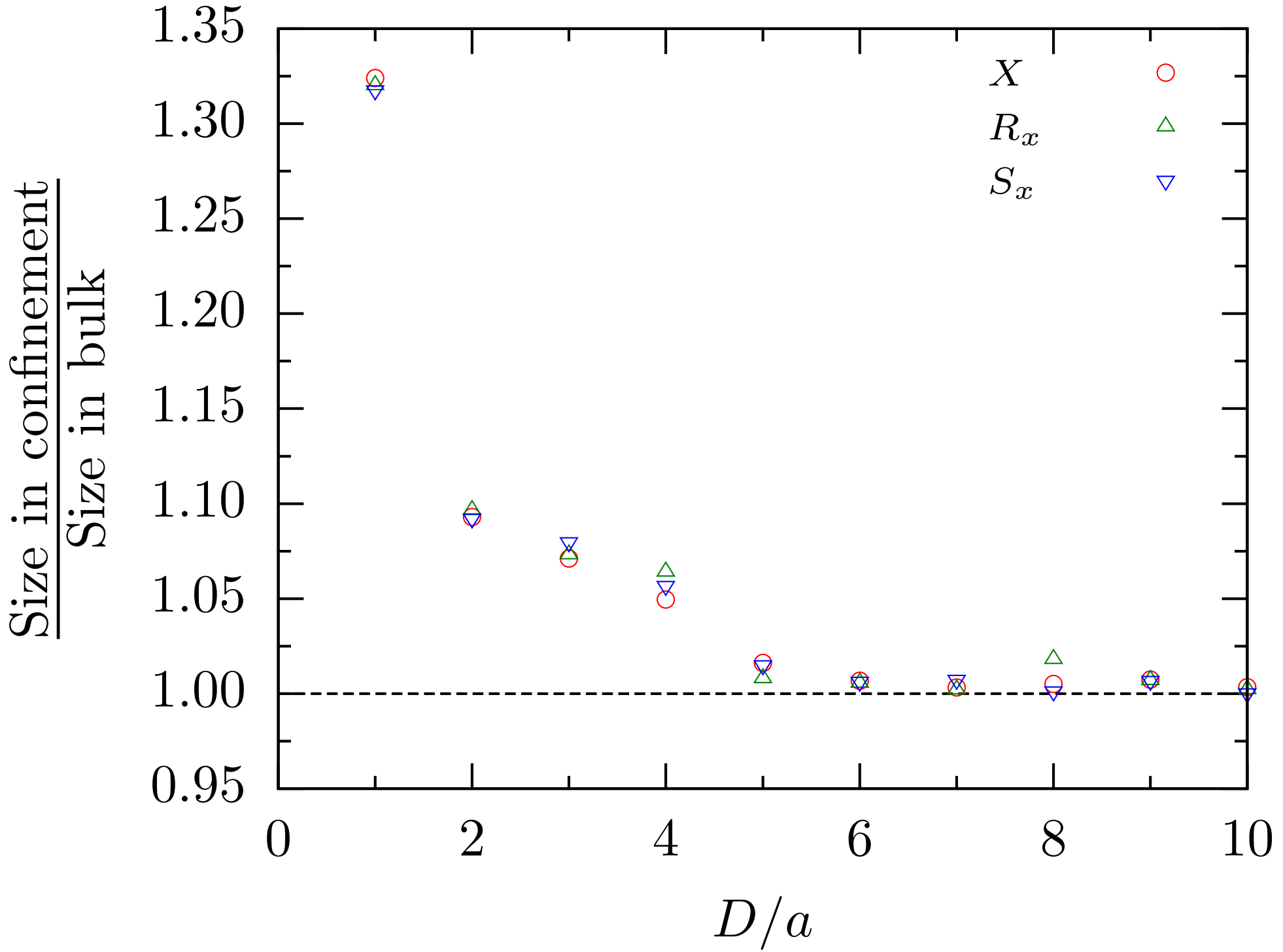
Size in confinement / Size in bulk
1.35
1.30
1.25
1.20
1.15
1.10
1.05
1.00
0.95
0
2
4
6
8
10
D/a
X
R_x
S_x

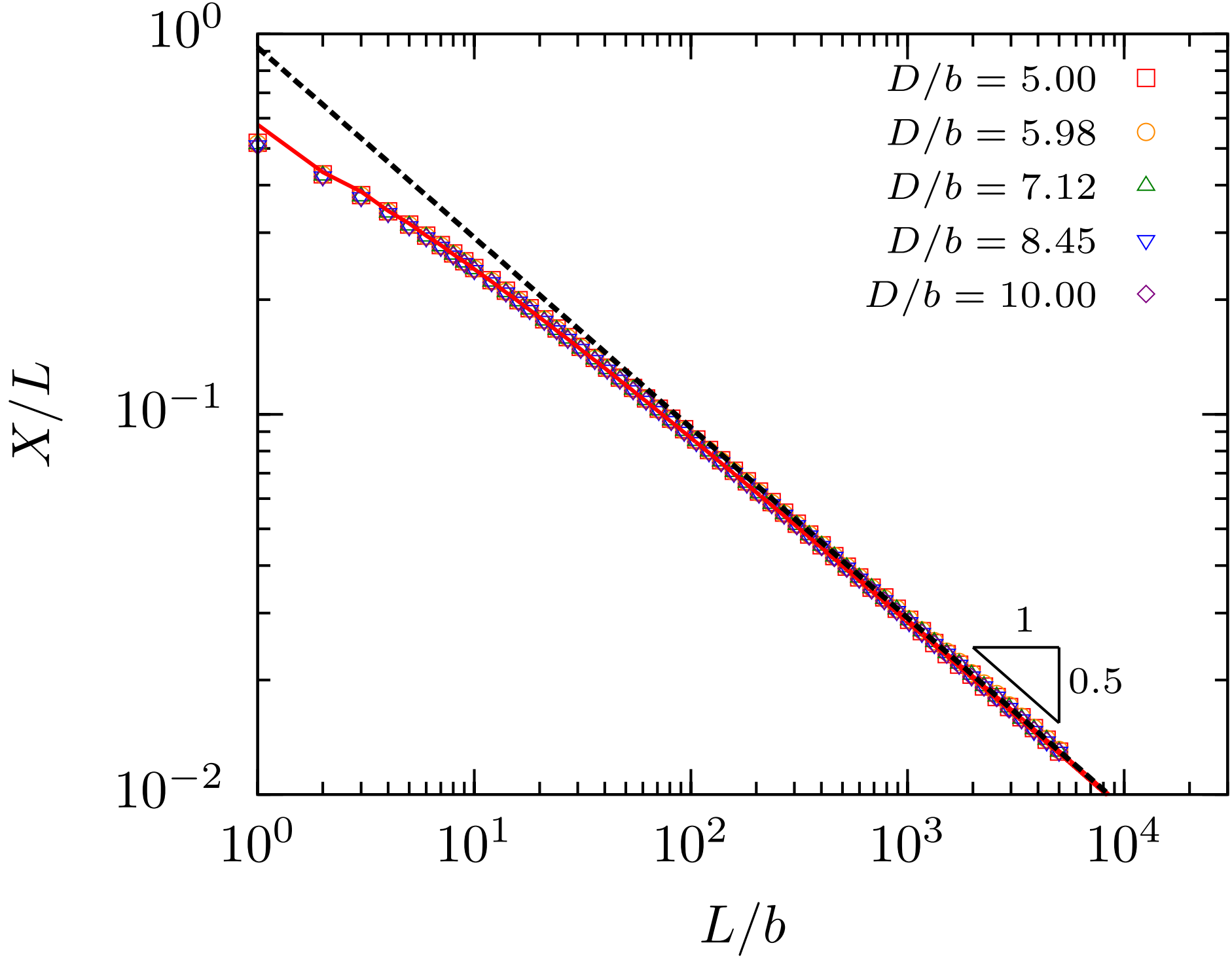
10^0
10^{-1}
10^{-2}
X/L
10^0
10^1
10^2
10^3
10^4
L/b
$D/b = 5.00$
$D/b = 5.98$
$D/b = 7.12$
$D/b = 8.45$
$D/b = 10.00$
1
0.5

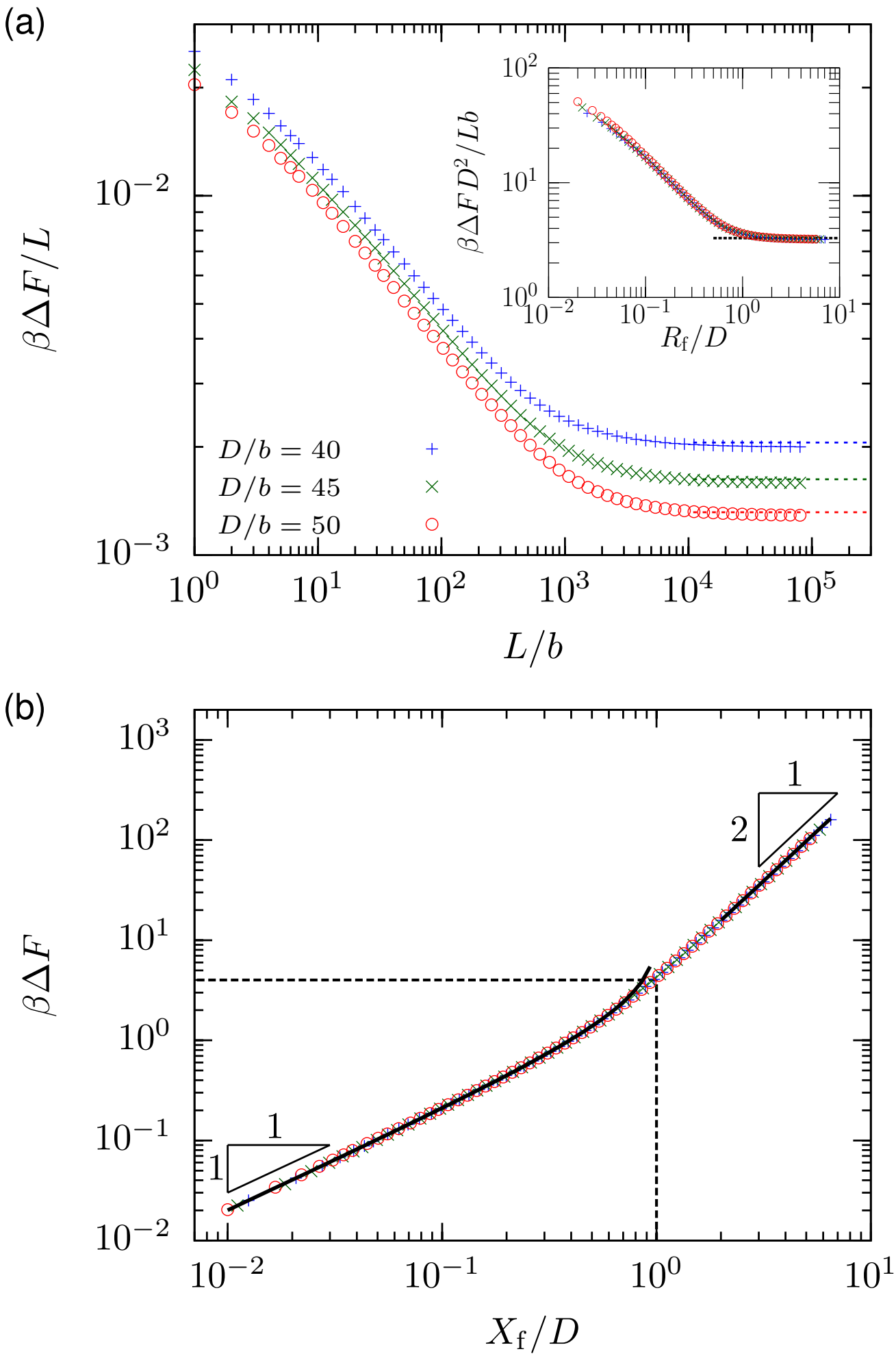
(a)
$\beta\Delta F/L$
L/b
$D/b = 40$
$D/b = 45$
$D/b = 50$
$\beta\Delta F D^2/Lb$
R_f/D
(b)
$\beta\Delta F$
X_f/D
1
2
1
1

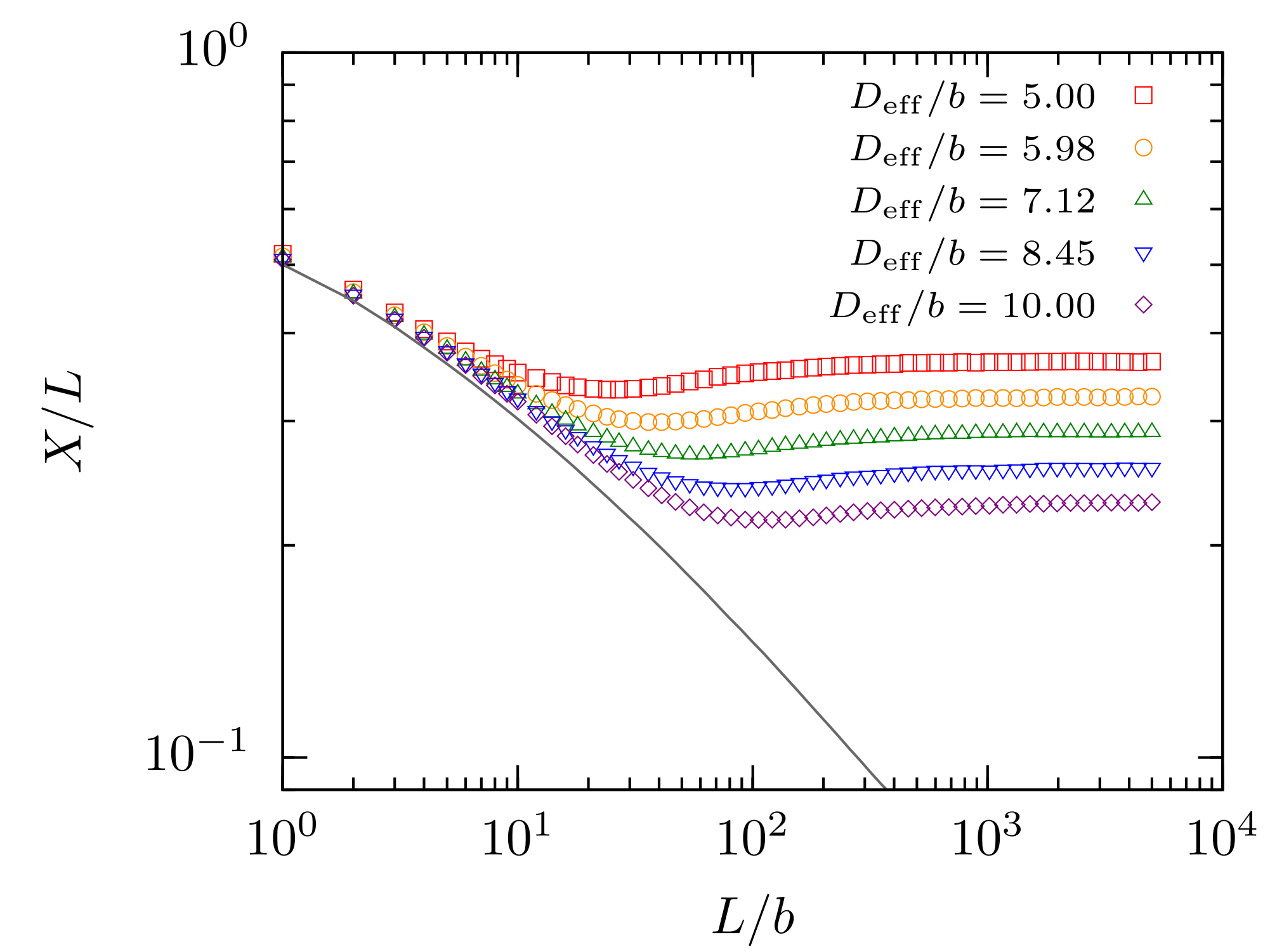
10^0
10^{-1}
X/L
10^0
10^1
10^2
10^3
10^4
L/b
$D_{\mathrm{eff}}/b = 5.00$
$D_{\mathrm{eff}}/b = 5.98$
$D_{\mathrm{eff}}/b = 7.12$
$D_{\mathrm{eff}}/b = 8.45$
$D_{\mathrm{eff}}/b = 10.00$

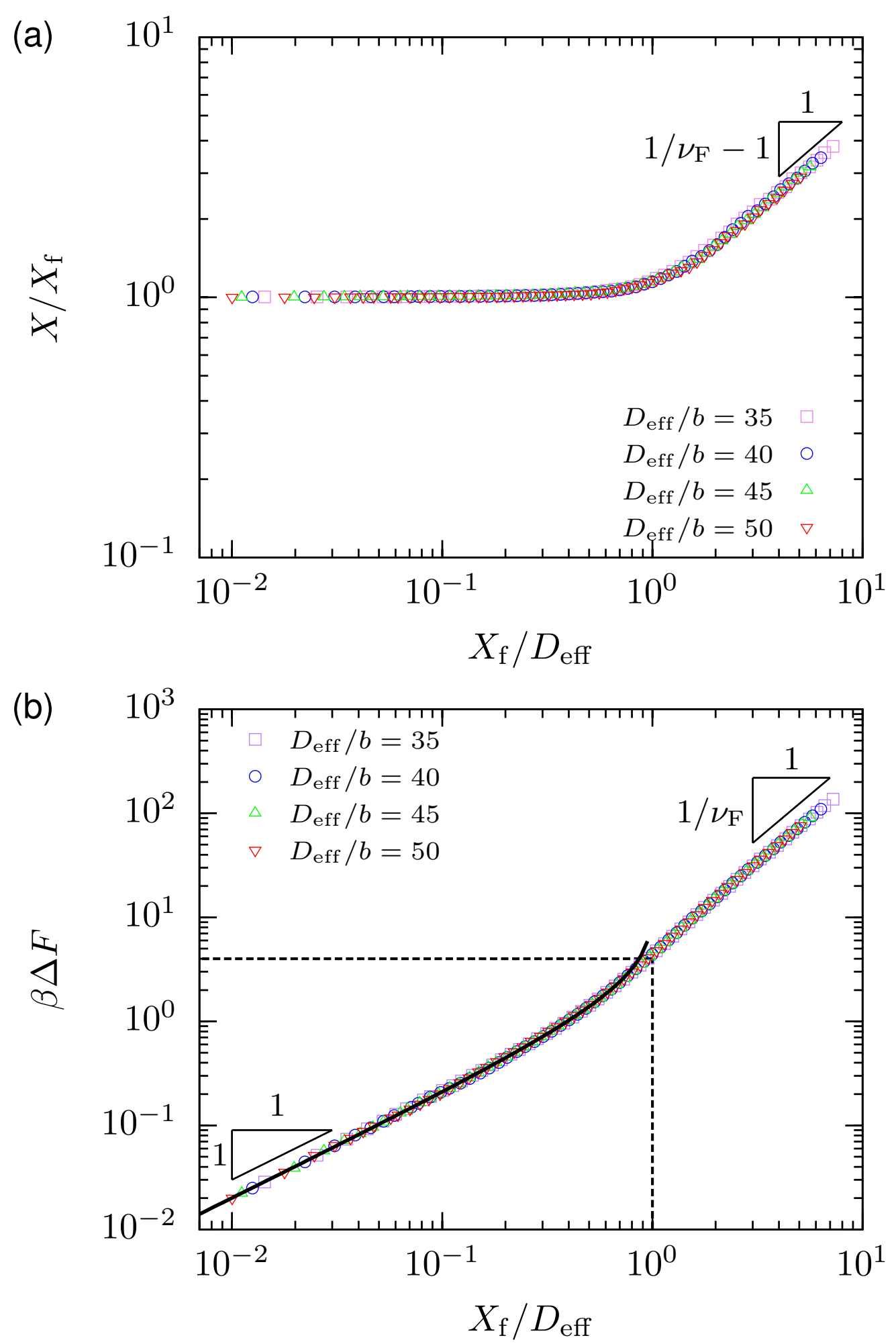
(a)
10^1
10^0
10^{-1}
X/X_f
1
$1/\nu_\mathrm{F} - 1$
$D_\mathrm{eff}/b = 35$
$D_\mathrm{eff}/b = 40$
$D_\mathrm{eff}/b = 45$
$D_\mathrm{eff}/b = 50$
10^{-2}
10^{-1}
10^0
10^1
$X_\mathrm{f}/D_\mathrm{eff}$
(b)
10^3
10^2
10^1
10^0
10^{-1}
10^{-2}
$\beta\Delta F$
$D_\mathrm{eff}/b = 35$
$D_\mathrm{eff}/b = 40$
$D_\mathrm{eff}/b = 45$
$D_\mathrm{eff}/b = 50$
1
$1/\nu_\mathrm{F}$
1
1
10^{-2}
10^{-1}
10^0
10^1
$X_\mathrm{f}/D_\mathrm{eff}$

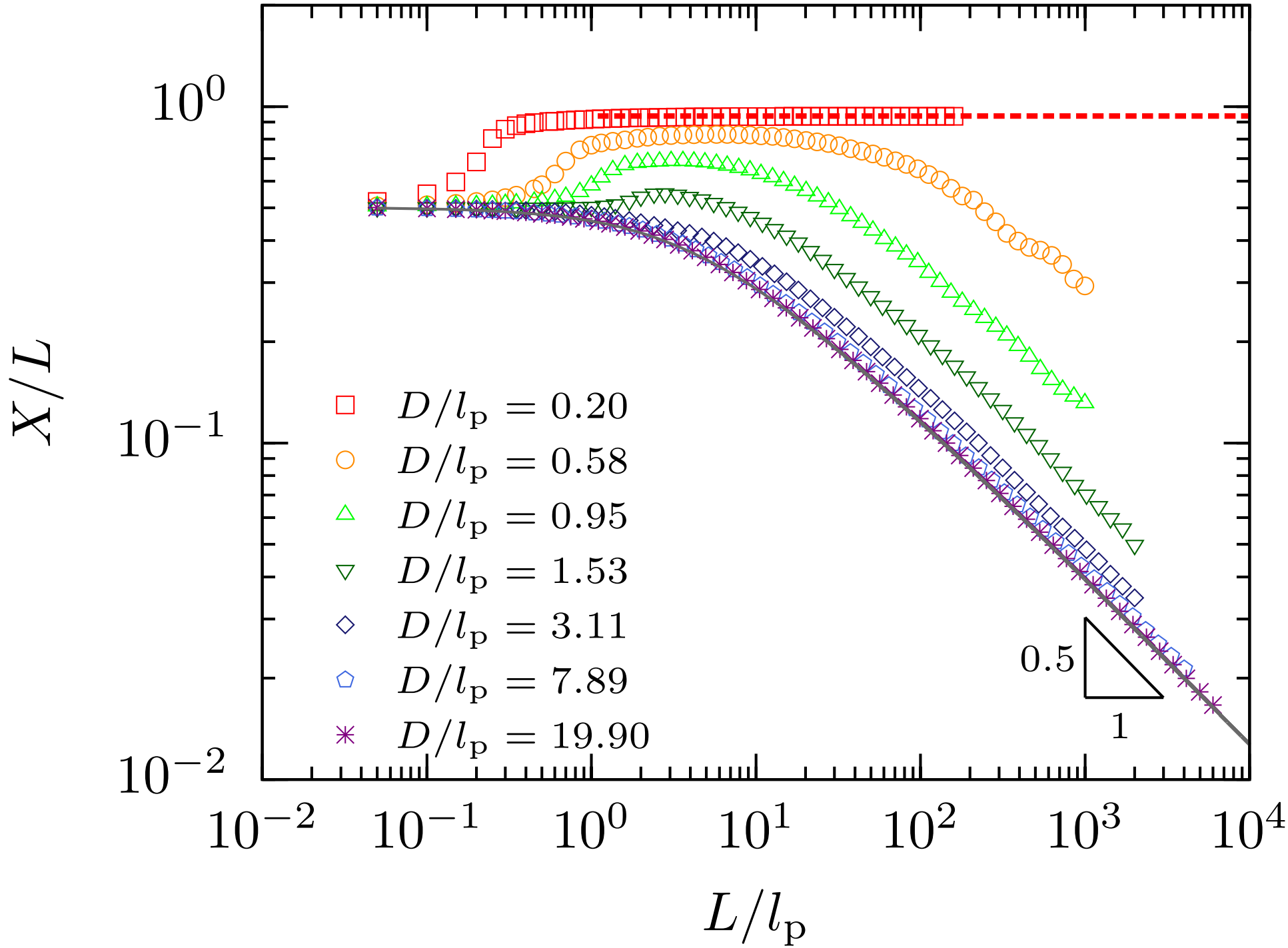
10^0
10^{-1}
10^{-2}
X/L
10^{-2}
10^{-1}
10^0
10^1
10^2
10^3
10^4
L/l_p
$D/l_\mathrm{p} = 0.20$
$D/l_\mathrm{p} = 0.58$
$D/l_\mathrm{p} = 0.95$
$D/l_\mathrm{p} = 1.53$
$D/l_\mathrm{p} = 3.11$
$D/l_\mathrm{p} = 7.89$
$D/l_\mathrm{p} = 19.90$
0.5
1

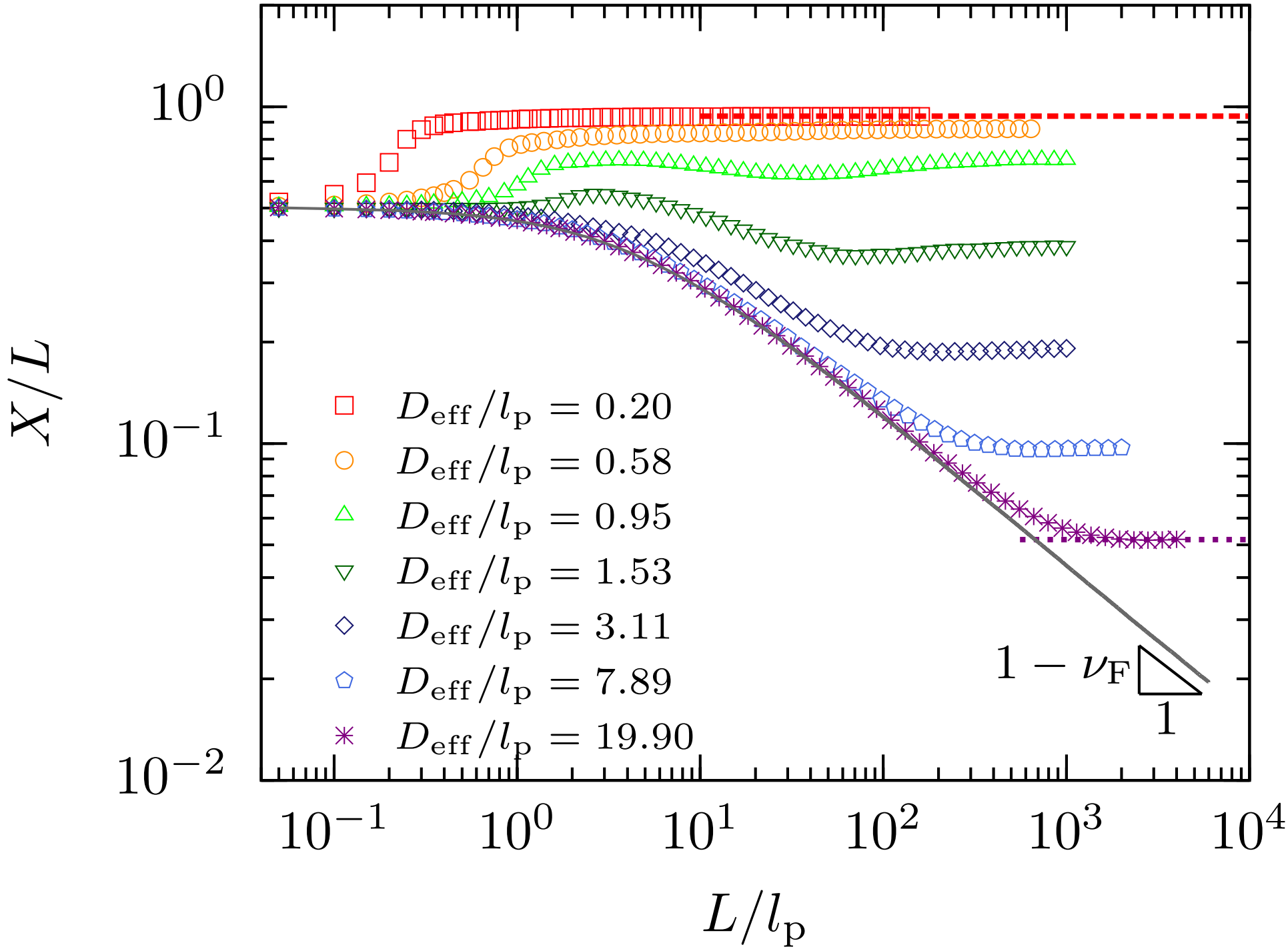
10^0
10^{-1}
10^{-2}
X/L
10^{-1}
10^0
10^1
10^2
10^3
10^4
L/l_p
$D_\mathrm{eff}/l_\mathrm{p} = 0.20$
$D_\mathrm{eff}/l_\mathrm{p} = 0.58$
$D_\mathrm{eff}/l_\mathrm{p} = 0.95$
$D_\mathrm{eff}/l_\mathrm{p} = 1.53$
$D_\mathrm{eff}/l_\mathrm{p} = 3.11$
$D_\mathrm{eff}/l_\mathrm{p} = 7.89$
$D_\mathrm{eff}/l_\mathrm{p} = 19.90$
$1 - \nu_\mathrm{F}$
1

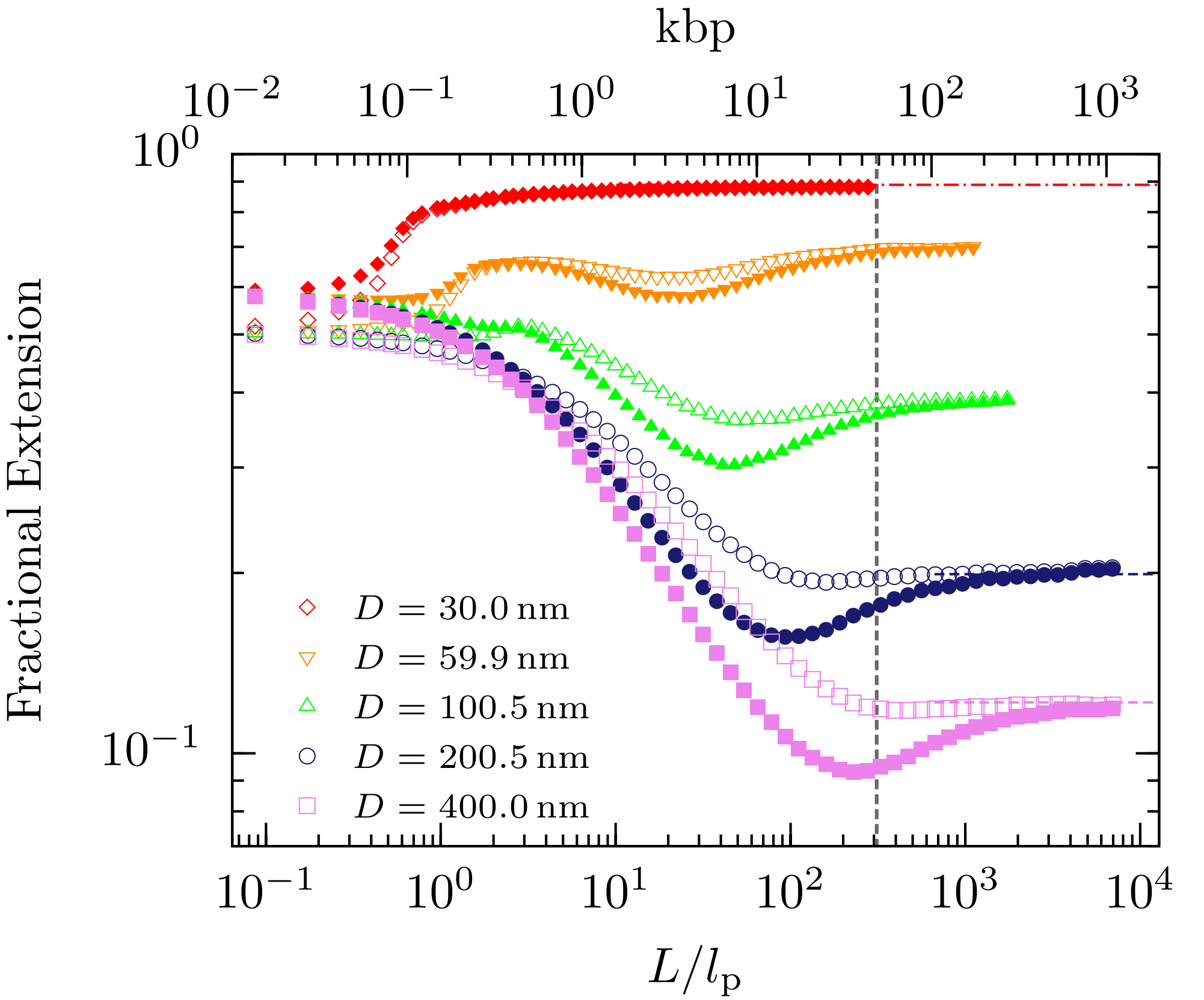
kbp
10^{-2}
10^{-1}
10^{0}
10^{1}
10^{2}
10^{3}
10^{0}
10^{-1}
Fractional Extension
$D = 30.0\,\mathrm{nm}$
$D = 59.9\,\mathrm{nm}$
$D = 100.5\,\mathrm{nm}$
$D = 200.5\,\mathrm{nm}$
$D = 400.0\,\mathrm{nm}$
10^{-1}
10^{0}
10^{1}
10^{2}
10^{3}
10^{4}
L/l_p